Ab initio semiclassical evaluation of vibrationally resolved electronic spectra with thawed Gaussians

Jiří Vaníček and Tomislav Begušić
Laboratory of Theoretical Physical Chemistry,
Institut des Sciences et Ingénierie Chimiques,
Ecole Polytechnique Fédérale de Lausanne (EPFL), CH-1015, Lausanne, Switzerland

(Dated: April 26, 2019)

Abstract

Vibrationally resolved electronic spectra of polyatomic molecules provide valuable information about the quantum properties of both electrons and nuclei. This chapter reviews the recent progress in *ab initio* semiclassical calculations of such spectra, based on the thawed Gaussian approximation and its extensions. After reviewing molecular quantum dynamics induced by the interaction with electromagnetic field and the most common semiclassical approximations to quantum dynamics, we explain details of the thawed Gaussian approximation and its variants. Next, we discuss the time-dependent approach to steady-state and time-resolved electronic spectroscopy, and review several standard models that facilitate interpreting vibrationally resolved electronic spectra. Finally, we present the on-the-fly *ab initio* implementation of the thawed Gaussian approximation and provide several examples of both linear and pump-probe spectra computed with this methodology, which, at a low additional cost and without sacrificing the ease of interpretation, outperforms the standard global harmonic approaches.

Keywords: absorption, stimulated emission, fluorescence, photoelectron spectrum, vibronic spectrum, Herzberg-Teller spectrum, Franck-Condon principle, Condon approximation, direct semiclassical dynamics, first-principles semiclassical dynamics

I. INTRODUCTION

Vibrationally resolved electronic spectroscopy provides a powerful tool for studying both electronic and nuclear motions in molecules: The measured spectrum contains precious information about the shapes of molecular potential energy surfaces, such as displacements between their minima, Duschinsky rotation between the normal modes of the ground-state and excited-state surfaces, couplings among vibrational modes, and nonadiabatic couplings between electronic states. The steady-state version of molecular electronic spectroscopy, used for many years, has been usually interpreted through the time-independent Franck–Condon picture, but an alternative, time-dependent approach (Heller, 1981b, 2018; Mukamel, 1999; Tannor, 2007), which examines the evolution of the nuclear wavepacket before evaluating the spectra, is more fundamental. The time-dependent approach is also much more natural for interpreting time-resolved spectra, and will be used exclusively in this chapter.

Accurate calculations of vibrationally resolved electronic spectra are difficult because they require both accurate potential energy surfaces, which necessitate expensive electronic structure calculations, and accurate nuclear quantum dynamics, impossible in high dimensions. As a result, such calculations are typically limited to accurate nuclear quantum dynamics calculations on potential energy surfaces which are either full-dimensional but approximate, such as those based on global harmonic models (Baiardi et al., 2013), or which take into account only a few degrees of freedom. To include all degrees of freedom as well as their anharmonicity without constructing global potential energy surfaces, various authors developed a number of trajectory-based on-the-fly *ab initio* (also called "direct dynamics" or "first-principles dynamics") quantum and semiclassical methods (Ceotto et al., 2009b; Curchod and Martínez, 2018; Gabas et al., 2017; Ianconescu et al., 2013; Richings et al., 2015; Saita and Shalashilin, 2012; Shalashilin and Child, 2004; Šulc et al., 2013; Tatchen and Pollak, 2009; Wong et al., 2011). Despite their success, which has, in fact, motivated the writing of this chapter, these methods are rather expensive when it comes to computing the vibrational structure of electronic spectra, since their convergence requires a large number of classical trajectories. In this chapter, we will, therefore, devote most attention to the on-the-fly *ab initio* version (Wehrle et al., 2014, 2015) of the thawed Gaussian approximation (TGA) (Heller, 1975), which provides a computationally efficient compromise between accurate but expensive multiple-trajectory semiclassical methods and cheap but restrictive and often flawed global harmonic methods. The TGA can be easily run in full dimensionality, and even its single-trajectory version captures some anharmonicity of the potential. Obviously, it cannot describe high resolution spectra, tunneling, wavepacket splitting, and very anharmonic dynamics in floppy molecules, yet, we will show several examples of surprisingly accurate molecular absorption, emission, and photoelectron spectra computed with the TGA.

Below, we define the notation and acronyms used in this chapter, the remainder of which is organized as follows: Section II, devoted to the quantum molecular dynamics induced by the interaction with electromagnetic field, introduces the most common approximations for the molecule-field interaction. Section III reviews briefly the most popular semiclassical approaches for solving the time-dependent Schrödinger equation. One of these, the thawed Gaussian approximation, is discussed in more detail, together with its extensions in Section IV. In Section V, the time-dependent approach to both steady-state and time-resolved spectra calculations is presented in the framework of approximations explained in Section II. We also discuss rotational averaging, important in describing electronic spectra beyond the Condon approximation but often ignored in theoretical calculations. In Section VI, several "standard" models useful for interpreting molecular electronic spectra are defined and accompanied with numerical examples demonstrating both their advantages and shortcomings. Intricacies of the on-the-fly *ab initio* implementation of the thawed Gaussian approximation are discussed in Section VII and several examples of absorption, emission, photoelectron, and pump-probe spectra computed with this approximation are presented in Section VIII. Finally, a conclusion and outlook are given in Section IX.

A. Notation

Throughout this chapter, we consider a molecular system with S relevant electronic states and D vibrational degrees of freedom. Electronic states are indexed by a Greek letter, such as $\alpha = 1, \ldots, S$, while vibrational modes are indexed by a Latin letter, such as $j = 1, \ldots, D$. Three different vector spaces play an important role in such systems: the ambient 3-dimensional space $\mathbb{R}^3$, the nuclear D-dimensional real coordinate space $\mathbb{R}^D$, and the electronic S-dimensional complex Hilbert space $\mathbb{C}^S$. To distinguish vectors and operators on these spaces, 3-dimensional vectors are denoted with an arrow (e.g., $\vec{\epsilon}$), nuclear D-dimensional vectors or $D \times D$ matrices use no special notation (e.g., generalized nuclear coordinates q), and the electronic S-dimensional vectors or $S \times S$ matrices (such as $\boldsymbol{\mu}$ or $\boldsymbol{A}$) representing electronic states or operators are denoted with the **bold** font. Scalar and matrix products in both the 3-dimensional and nuclear D-dimensional spaces are denoted with a dot (as in $\vec{\mu}_{21} \cdot \vec{\epsilon}$ or $p^T \cdot m^{-1} \cdot p$), whereas the matrix product in the electronic Hilbert space use no special notation; it is expressed by a juxtaposition of matrices (as in $\boldsymbol{AB}$). Finally, the nuclear operators are denoted with a hat $\hat{}$ (as in $\hat{p}$). The ground vibrational state g of the ground electronic state 1 is denoted by $|1, g\rangle$. Angular frequency of light ω is used in all expressions, while the numerical results are displayed in terms of the wavenumber $\tilde{\nu} = \omega/(2\pi c)$.

B. List of acronyms

3TGA	three thawed Gaussians approximation
CASPT2	complete active space second-order perturbation theory
CCSD	coupled cluster singles and doubles
ETGA	extended thawed Gaussian approximation
MP2	Møller-Plesset second-order perturbation theory
n-TGA	n thawed Gaussians approximation
TGA	thawed Gaussian approximation

II. MOLECULAR QUANTUM DYNAMICS INDUCED BY THE INTERACTION WITH ELECTROMAGNETIC FIELD

Vibrationally resolved electronic spectra reflect the molecular motion following electronic excitations induced by the interaction with visible or ultraviolet electromagnetic field. Such an electronic excitation can induce nonadiabatic dynamics between different electronic states, but we will assume the validity of the Born-Oppenheimer approximation, which will allow us to focus on adiabatic dynamics, i.e., dynamics on a single Born-Oppenheimer potential energy surface because many interesting phenomena in continuous-wave electronic spectroscopy depend only on dynamics on a single surface. Likewise, in time-resolved spectroscopy with well-separated ultrashort pulses, one can get rather far by considering only a sequence of such elementary steps, each of which takes place on a single surface. Therefore, we will not cover nonadiabatic dynamics here and instead refer the interested reader to various books and reviews of this vast subject (Baer, 2006; Bircher et al., 2017; Domcke and Stock, 1997; Domcke and Yarkony, 2012; Levine and Martinez, 2007; Mukamel, 2000; Nakamura, 2012; Ryabinkin et al., 2017).

A. Exact dynamics, electric dipole approximation, and quasiresonant condition

To justify our focus on electronically adiabatic dynamics we start the discussion with the full molecular wavefunction that involves both electronic and nuclear degrees of freedom. This will be useful because all our applications come from electronic spectroscopy, where the electromagnetic field induces the transition of the molecule to a different electronic state; this transition is followed by nuclear adiabatic dynamics on the corresponding, new potential energy surface.

The simplest electronic transition involves only two electronic states and, in this two-

dimensional electronic basis, the time-dependent molecular wavepacket can be written as

$$\boldsymbol{\psi}(t) = \begin{pmatrix} |\psi_1(t)\rangle \\ |\psi_2(t)\rangle \end{pmatrix}, \tag{1}$$

where $|\psi_\alpha(t)\rangle$ is a time-dependent nuclear wavepacket moving on the αth potential energy surface. Evolution of $\boldsymbol{\psi}(t)$ is determined by the time-dependent molecular Schrödinger equation

$$\mathrm{i}\hbar\frac{\mathrm{d}}{\mathrm{d}t}\boldsymbol{\psi}(t) = \hat{\boldsymbol{H}}_{\mathrm{full}}(t)\boldsymbol{\psi}(t), \tag{2}$$

driven by the "full" time-dependent Hamiltonian

$$\hat{\boldsymbol{H}}_{\mathrm{full}}(t) = \hat{\boldsymbol{H}} + \hat{\boldsymbol{V}}_{\mathrm{int}}(t), \tag{3}$$

where $\hat{\boldsymbol{H}}$ is the time-independent molecular Hamiltonian and $\hat{\boldsymbol{V}}_{\mathrm{int}}(t)$ the interaction potential of the molecule with the electromagnetic field. The exact solution of Eq. (2), which can be formally written as

$$\boldsymbol{\psi}(t) = \mathcal{T}\exp\left[-\frac{\mathrm{i}}{\hbar}\int_{t_0}^{t}\hat{\boldsymbol{H}}_{\mathrm{full}}(t')\,\mathrm{d}t'\right]\boldsymbol{\psi}(t_0), \tag{4}$$

where $\mathcal{T}$ is the time-ordering operator, is greatly simplified by invoking the following approximations.

Within the *electric dipole approximation* (Schatz and Ratner, 2002), the interaction potential is given by

$$\hat{\boldsymbol{V}}_{\mathrm{int}}(t) = -\hat{\vec{\boldsymbol{\mu}}}\cdot\vec{E}(t), \tag{5}$$

where $\hat{\vec{\boldsymbol{\mu}}}$ is the molecular electric transition dipole moment and $\vec{E}(t)$ the electric field at the location of the molecule. This approximation requires the wavelength of the electromagnetic field to be longer than the size of the molecule, which is quite well justified for medium size molecules and visible light.

We further assume that there are no nonadiabatic or spin-orbit couplings between the two electronic states and, as a consequence, that the only electronic transitions are induced by the interaction with the electromagnetic field. This so-called *Born-Oppenheimer approximation* implies that the molecular Hamiltonian $\hat{\boldsymbol{H}}$ is a diagonal S-dimensional matrix $\mathrm{diag}(\hat{H}_1,\ldots,\hat{H}_S)$. To rigorously justify neglecting nonadiabatic or spin-orbit couplings, several criteria (Baer, 2006; Bircher et al., 2017; Domcke and Yarkony, 2012; Nakamura, 2012) can be used, starting from static criteria such as the size of the energy gap between electronic states or the strength of nonadiabatic couplings, to more dynamical criteria such as the population dynamics. Among the most rigorous dynamical criteria, "adiabaticity"(MacKenzie et al., 2012; Zimmermann and Vaníček, 2010; Zimmermann and Vaníček, 2012a,b) is defined as the overlap of the adiabatically and nonadiabatically evolved molecular wavefunctions: If adiabaticity is close to 1, the nonadiabatic effects can be safely neglected, whereas if adiabaticity is much smaller than 1, they must be included in the simulation. Although rigorous,

this criterion by itself would not be very practical; fortunately, there exist efficient approximate semiclassical methods to estimate the adiabaticity without solving the full Schrödinger equation (2) exactly (Zimmermann and Vaníček, 2010; Zimmermann and Vaníček, 2012a,b).

A visible or ultraviolet electromagnetic field will excite electronic transitions, and if it is approximately in resonance with the transition from state 1 to state 2, we are allowed to retain only the off-diagonal elements of the transition dipole moment:

$$\hat{\vec{\boldsymbol{\mu}}} \approx \begin{pmatrix} 0 & \hat{\vec{\mu}}_{12} \\ \hat{\vec{\mu}}_{21} & 0 \end{pmatrix}. \tag{6}$$

This is a special case of the *quasiresonant condition* [see Marquardt and Quack (1989); Quack (1978, 1979); Quack and Sutcliffe (1985)].

B. Perturbation theory, zero-temperature and Condon approximations

If the electromagnetic field is strong, one must treat it explicitly and worry about the coupled dynamics on the two surfaces at least during the excitation process; in other words, one must evolve the two-component state $\boldsymbol{\psi}(t)$. For sufficiently weak fields or for short interaction times, one may employ the *time-dependent perturbation theory*. Whereas the first-order perturbation theory is often sufficient for linear spectroscopy, the second order is required, e.g., for resonance Raman spectroscopy and the third or higher order for more sophisticated nonlinear and time-resolved spectroscopic techniques (Mukamel, 1999).

Within the first-order perturbation theory, the molecular state evolves as

$$\boldsymbol{\psi}(t) = \hat{\boldsymbol{U}}(t)\boldsymbol{\psi}(0) - \frac{\mathrm{i}}{\hbar}\int_{-\infty}^{t} \mathrm{d}t' \hat{\boldsymbol{U}}(t-t')\hat{\boldsymbol{V}}_{\mathrm{int}}(t')\hat{\boldsymbol{U}}(t')\boldsymbol{\psi}(0), \tag{7}$$

where $\hat{\boldsymbol{U}}(t) = \exp\left(-\mathrm{i}\hat{\boldsymbol{H}}t/\hbar\right)$ denotes the molecular evolution operator in the absence of the electromagnetic field. For electronic transitions, expression (7) simplifies; the only interesting part is the first-order term describing the wavepacket generated by the field on the second potential energy surface:

$$|\psi_2(t)\rangle = \frac{\mathrm{i}}{\hbar}\int_{-\infty}^{t} \mathrm{d}t' \hat{U}_2(t-t')\hat{\vec{\mu}}_{21} \cdot \vec{E}(t')\hat{U}_1(t')|\psi_1(0)\rangle, \tag{8}$$

This equation implies that the initial state first evolves freely on the first surface, then, at time t', interacts with the field, which induces instantaneously an electronic transition to the second electronic state, and, finally, evolves for the remaining time on the second surface. The total wavepacket generated in the excited state is obtained by integrating this elementary process over all possible interaction times t'. In practical terms, since $\hat{U}_\alpha(t) = \exp(-\mathrm{i}\hat{H}_\alpha t/\hbar)$ is the nuclear evolution operator on surface α, one only has to solve the

nuclear Schrödinger equation

$$\mathrm{i}\hbar\frac{\mathrm{d}}{\mathrm{d}t}|\phi(t)\rangle = \hat{H}_\alpha|\phi(t)\rangle \tag{9}$$

with a time-independent Hamiltonian $\hat{H}_\alpha$ and general initial state $|\phi(0)\rangle$ instead of the more complicated molecular equation (2) with a time-dependent Hamiltonian. The solution of Eq. (9) can be written formally as

$$|\phi(t)\rangle = \exp\left(-\mathrm{i}\hat{H}_\alpha t/\hbar\right)|\phi(0)\rangle. \tag{10}$$

At room temperature, most of the molecules are typically in the vibrational ground state $|1,g\rangle$ of the ground electronic state, which is, in particular, an eigenstate of $\hat{H}_1$, hence, the first evolution operator $\hat{U}_1(t')$ yields only a phase factor $\exp(-\mathrm{i}E_{1,g}t/\hbar)$, the only effect of which is an overall shift of the electronic spectrum by the zero-point vibrational energy $E_{1,g}$ of the initial potential energy surface (we will show this explicitly below). As a result, in the case of electronic transitions, the only interesting dynamics occurs after time t', in the second electronic state, and hence, as promised, the problem reduces to adiabatic dynamics on the second surface. The assumption that the initial state is a vibrational ground state of $\hat{H}_1$ is usually referred to as the *zero-temperature approximation* and avoids the necessity of Boltzmann averaging over different initial states. It is a good approximation for vibrationally resolved electronic spectroscopy. [Note that we anticipated the low-temperature approximation already in Eq. (1) by focussing our attention to pure states of the molecule. This is justified as long as we are not interested in rotationally resolved spectra, which would, at room temperature, necessitate a density operator treatment.]

Finally, one also frequently makes the *Condon approximation* (Condon, 1927, 1928; Franck and Dymond, 1926), which amounts to ignoring the dependence of the transition dipole on nuclear coordinates: $\vec{\mu}_{12}(q) \approx \text{const} = \vec{\mu}_{12}$. Note that removing the coordinate dependence from $\vec{\mu}_{12}(q)$ permits taking the product $\hat{\vec{\mu}}_{21} \cdot \vec{E}(t')$ outside of the integral over $\mathrm{d}t'$ in Eq. (8).

III. SEMICLASSICAL APPROXIMATION TO QUANTUM DYNAMICS

Approximations for treating the molecule-field interaction, which were discussed in the previous section, simplify the solution of the time-dependent Schrödinger equation (2). Unfortunately, even after making these approximations, the quantum propagation of a wavefunction of a large molecule is impossible due to the exponential scaling of the computational cost with dimensionality. In addition, quantum dynamics requires construction of global potential energy surfaces, which is another task scaling exponentially with dimensions.

Semiclassical trajectory-based methods circumvent these two challenges and thus provide an interesting alternative for molecular dynamics simulations. On one hand, the propagation of classical trajectories requires only local knowledge of the potential energy surfaces,

allowing on-the-fly evaluation of necessary ab initio data. On the other hand, and in contrast to even simpler classical molecular dynamics, semiclassical trajectories carry along phases, and as a result can approximately describe nuclear quantum effects, such as the zero-point energy and quantum coherence. Many semiclassical methods have been proposed in the literature; here we can mention only a few, and therefore we focus on those that have been combined with *ab initio* evaluation of the electronic structure.

Probably the simplest semiclassical method is the single-trajectory *thawed Gaussian approximation* (Heller, 1975, 2018), in which the quantum wavepacket is approximated by a single Gaussian whose center moves along a classical trajectory. Because it has a finite nonzero width and because it is allowed to rotate and stretch in phase space, the thawed Gaussian captures some quantum effects. The TGA, however, obviously cannot describe wavepacket splitting, and therefore is expected to be valid only for rather short times and describe only low or medium resolution spectra. Below, we will discuss in detail various extensions and present several on-the-fly *ab initio* applications of this method, and hopefully surprise the reader by the usefulness of the TGA in electronic spectroscopy.

Wavepacket splitting and full anharmonicity of the potential can be captured by multi-trajectory methods, such as the *initial value representation* (Miller, 1970, 2001) or the *frozen Gaussian approximation* (Heller, 1981a), in which the propagated wavepacket is represented by an ensemble of rigid Gaussians. The two concepts are merged in one of the most accurate semiclassical approximations, the *Herman–Kluk* initial value representation (Herman and Kluk, 1984; Kay, 2005; Miller, 2001), which can be derived from the stationary-phase approximation to the Feynman path integral propagator. In the Herman-Kluk initial value representation, the nuclear quantum evolution operator, $\hat{U}(t) = \exp(-\mathrm{i}\hat{H}t/\hbar)$, needed in evaluating Eq. (8), is approximated as

$$e^{-\mathrm{i}\hat{H}t/\hbar} \approx h^{-D} \int \mathrm{d}q_0 \mathrm{d}p_0 \; R_t(q_0,p_0) e^{\mathrm{i}S_t(q_0,p_0)/\hbar} |q_t p_t\rangle\langle q_0 p_0|, \tag{11}$$

where (q_t, p_t) denote the phase-space coordinates at time t of a point along the classical trajectory and $S_t(q_0, p_0)$ is the corresponding classical action. In the position representation, Glauber's canonical coherent states $|q_t p_t\rangle$ (Glauber, 1963) from Eq. (11) are Gaussians

$$\langle q|q_t p_t\rangle = \left(\frac{\det g}{\pi^D}\right)^{1/4} \exp\left[-\frac{1}{2}(q-q_t)^T \cdot g \cdot (q-q_t) + \frac{\mathrm{i}}{\hbar} p_t^T \cdot (q-q_t)\right], \tag{12}$$

with a time-independent $D \times D$ width matrix g,

$$R_t(q_0,p_0) = \sqrt{\det\left[\frac{1}{2}\left(M_{t,qq} + g^{-1}\cdot M_{t,pp}\cdot g - \mathrm{i}\hbar M_{t,qp}\cdot g + \frac{\mathrm{i}}{\hbar} g^{-1}\cdot M_{t,pq}\right)\right]} \tag{13}$$

is the Herman–Kluk prefactor, and symbols $M_{t,xy} = \partial x_t/\partial y_0$ represent the four $D \times D$

sub-blocks of the $2D \times 2D$ stability matrix

$$M_t = \begin{pmatrix} M_{t,qq} & M_{t,qp} \\ M_{t,pq} & M_{t,pp} \end{pmatrix} := \begin{pmatrix} \frac{\partial q_t}{\partial q_0} & \frac{\partial q_t}{\partial p_0} \\ \frac{\partial p_t}{\partial q_0} & \frac{\partial p_t}{\partial p_0} \end{pmatrix}. \tag{14}$$

Note that the form of the coherent state wavefunctions in Eq. (12) differs from that of Klauder (Child and Shalashilin, 2003; Klauder and Skagerstam, 1985) by a factor $\exp(ip_t q_t/2\hbar)$, which modifies the action S_t but leaves the classical equations of motion for q_t and p_t unchanged. The phase-space integral in Eq. (11) is usually evaluated by sampling the initial conditions of classical trajectories using Monte Carlo techniques; the subsequent propagation requires computing the potential energy V to evolve the action S, the force (i.e., $-\operatorname{grad} V$) to evolve positions and momenta, and the Hessian of V to evolve the stability matrix M_t.

Despite some progress, the application of the Herman–Kluk initial value representation to large systems is difficult. First, the oscillatory nature of the integrand in Eq. (11) implies that a very large number of trajectories is required to converge the results. Second, calculating the Hessian is much more expensive than evaluating the force needed in classical *ab initio* molecular dynamics. The computational cost can be reduced by invoking various additional approximations, such as the prefactor-free propagator (Zhang and Pollak, 2003), time averaging (Kaledin and Miller, 2003), and Filinov filtering (cellularization) (Heller, 1991; Makri and Miller, 1988; Walton and Manolopoulos, 1996), which has been used to improve Monte Carlo statistics (Church et al., 2017; Walton and Manolopoulos, 1996; Wang et al., 2001) and to derive new approximate semiclassical methods (Antipov et al., 2015; Church et al., 2017; Thoss et al., 2001; Šulc and Vaníček, 2012; Zambrano et al., 2013). Thanks to these acceleration techniques, the Herman-Kluk propagator has been successfully merged with on-the-fly dynamics and used to calculate vibrationally resolved spectra (Ceotto et al., 2009a,b; Tatchen and Pollak, 2009; Wong et al., 2011) and internal conversion rates (Ianconescu et al., 2013). Time averaging has proved useful in on-the-fly simulations as a central ingredient of the multiple-coherent-states time-averaged semiclassical initial value representation (Ceotto et al., 2009a,b, 2011). This method is especially well suited for the determination of vibrational frequencies and prediction of vibrational spectra (Buchholz et al., 2016; Ceotto et al., 2011, 2013; Gabas et al., 2017). A clever choice of the initial coherent states allows a drastic reduction of the number of trajectories required for convergence of desired spectral regions.

Both the thawed Gaussian approximation and various forms of the initial value representation are general methods for approximating quantum dynamics and are exact in arbitrary harmonic systems, but most require the knowledge of the potential Hessian along the trajectory. In the case of electronic spectroscopy, which is the main subject of this chapter, there is a class of methods that only require the force, and not the Hessian of the potential, but at a cost of being exact only for displaced harmonic systems. These closely related

methods are known as the phase averaging (Mukamel, 1982, 1999), Wigner averaged classical limit (Egorov et al., 1998, 1999), linearized semiclassical initial value representation (Shi and Geva, 2005), or dephasing representation (Vaníček, 2004, 2006; Zambrano et al., 2013).

IV. THAWED GAUSSIAN APPROXIMATION

The main goal of this chapter is to demonstrate the power of on-the-fly *ab initio* semiclassical dynamics in electronic spectroscopy on the example of the thawed Gaussian approximation. Let us, therefore, discuss this method and its extensions in more detail.

A. Thawed Gaussian approximation

The TGA (Heller, 1975) relies on the fact that a Gaussian wavepacket propagated exactly quantum-mechanically in an arbitrary time-dependent harmonic potential remains Gaussian. The TGA improves on the frequently used global harmonic models (discussed below, in Section VI A) by approximating the potential energy surface to the second order only locally, in what is known as the *local harmonic approximation*. Although approximating the initial state in electronic spectroscopy with a Gaussian is only reasonable within the Condon approximation, let us first discuss this simplest case because it will serve as a starting point for extensions to more general forms of the initial wavepacket needed to describe Herzberg–Teller spectra.

A general D-dimensional Gaussian wavepacket at time t can be written in the position representation as

$$\psi(q,t) = N_0 \exp\left\{\frac{\mathrm{i}}{\hbar}\left[\frac{1}{2}(q-q_t)^T\cdot A_t\cdot(q-q_t) + p_t^T\cdot(q-q_t) + \gamma_t\right]\right\}, \tag{15}$$

where $N_0 = [\det(\mathrm{Im}A_0/\pi\hbar)]^{1/4}$ is a normalization constant, (q_t, p_t) are the phase-space coordinates of the center of the wavepacket, A_t is a symmetric complex width matrix, and γ_t a complex number whose real part is a dynamical phase and imaginary part guarantees the normalization at times $t > 0$. The wavepacket is propagated with an effective Hamiltonian

$$\hat{H}_{\mathrm{eff}}(t) \equiv H_{\mathrm{eff}}(\hat{q},\hat{p},t) = \frac{1}{2}\hat{p}^T\cdot m^{-1}\cdot\hat{p} + V_{\mathrm{eff}}(\hat{q},t), \tag{16}$$

where $m = \mathrm{diag}(m_1,\ldots,m_D)$ is the diagonal mass matrix and V_{eff} an effective time-dependent potential given by the local harmonic approximation of the true potential V at the center of the wavepacket:

$$V_{\mathrm{eff}}(q,t) = V|_{q_t} + (\mathrm{grad}_q V|_{q_t})^T\cdot(q-q_t) + \frac{1}{2}(q-q_t)^T\cdot\mathrm{Hess}_q V|_{q_t}\cdot(q-q_t). \tag{17}$$

In this equation, $(\mathrm{grad}_q V)_i := \partial_{q_i} V$ is the gradient of V and $(\mathrm{Hess}_q V)_{ij} := \partial_{q_i}\partial_{q_j} V$ is the symmetric Hessian matrix of V. Insertion of the wavepacket ansatz (15) and the effective potential (17) into the nuclear time-dependent Schrödinger equation (9) yields a system of ordinary differential equations for the time-dependent parameters of the Gaussian (Heller, 1975):

$$\dot{q}_t = m^{-1} \cdot p_t \,, \tag{18}$$

$$\dot{p}_t = -\,\mathrm{grad}_q V|_{q_t} \,, \tag{19}$$

$$\dot{A}_t = -A_t \cdot m^{-1} \cdot A_t - \mathrm{Hess}_q V|_{q_t} \,, \tag{20}$$

$$\dot{\gamma}_t = L_t + \frac{\mathrm{i}\hbar}{2} \mathrm{Tr}\left(m^{-1} \cdot A_t\right). \tag{21}$$

In the last equation, L_t denotes the Lagrangian

$$\begin{aligned} L_t &= \frac{1}{2}\dot{q}_t^T \cdot m \cdot \dot{q}_t - V\left(q_t\right) \\ &= \frac{1}{2} p_t^T \cdot m^{-1} \cdot p_t - V\left(q_t\right). \end{aligned} \tag{22}$$

The system of differential equations (18)-(21), which is within the local harmonic approximation equivalent to the solution of the Schrödinger equation (9), implies that phase-space coordinates q_t and p_t follow classical Hamilton's equations of motion, while the propagation of the width A_t and phase γ_t involves propagating the $2D \times 2D$ stability matrix (14), and therefore requires evaluating the Hessians of the potential energy surface V.

B. Propagation of the parameters of the thawed Gaussian wavepacket

Equations (18)–(19) for the position and momentum are classical Hamilton's equations of motion for Hamiltonian $H(q,p)$, so q_t and p_t can be readily propagated with the Verlet algorithm or other symplectic integrators. Solving equations (20)-(21) for the width matrix A_t and generalized phase γ_t is more complicated. The approach by Heller (1976) and Hagedorn (1980) [see also (Lee and Heller, 1982) and (Faou et al., 2009)] suggests splitting the complex symmetric width matrix A_t into a product of two complex $D \times D$ matrices P_t and Q_t:

$$A_t = P_t \cdot Q_t^{-1}, \tag{23}$$

$$P_t = m \cdot Q_t. \tag{24}$$

Differential equations for Q_t and P_t, obtained from Eqs. (20), (23), and (24),

$$\dot{Q}_t = m^{-1} \cdot P_t, \tag{25}$$

$$\dot{P}_t = -\mathrm{Hess}_q V|_{q_t} \cdot Q_t, \tag{26}$$

can be interpreted as Hamilton's equations of motion of the Hamiltonian

$$H_{\mathrm{sc}}(Q,P;q_t) = \frac{1}{2}\,\mathrm{Tr}\left[P^\dagger\cdot m^{-1}\cdot P + Q^\dagger\cdot \mathrm{Hess}_q V|_{q_t}\cdot Q\right], \tag{27}$$

which depends on time through the parameter q_t. The solution can then be written explicitly in terms of the stability matrix M_t:

$$\begin{pmatrix} Q_t \\ P_t \end{pmatrix} = M_t \begin{pmatrix} Q_0 \\ P_0 \end{pmatrix}; \tag{28}$$

In other words, Q_t and P_t are solutions of a linear Hamiltonian system, obtained by linearizing the original system about the center of the thawed Gaussian. Choosing the initial values as $Q_0 = (2\,\mathrm{Im}\,A_0/\hbar)^{-1/2}$ and $P_0 = A_0\cdot Q_0$ guarantees, in addition, that the sum $H(q_t,p_t) + H_{\mathrm{sc}}(Q_t,P_t)$ equals the total energy of the thawed Gaussian wavepacket (Begušić et al., 2019).

As for γ_t, which is a generalization of classical action and represents both the dynamical phase and normalization, it is evaluated as

$$\gamma_t = \gamma_0 + \int_0^t L_\tau \mathrm{d}\tau + \frac{\mathrm{i}\hbar}{2}\int_0^t \mathrm{Tr}\left(m^{-1}\cdot A_\tau\right)\mathrm{d}\tau \tag{29}$$

$$= \gamma_0 + \int_0^t L_\tau \mathrm{d}\tau + \frac{\mathrm{i}\hbar}{2}\int_0^t \mathrm{Tr}\left(\dot{Q}_\tau\cdot Q_\tau^{-1}\right)\mathrm{d}\tau \tag{30}$$

$$= \gamma_0 + \int_0^t L_\tau \mathrm{d}\tau + \frac{\mathrm{i}\hbar}{2}\ln\left(\det Q_t\right), \tag{31}$$

where the conditions imposed on Q and P are used in order to obtain the final expression. Because the determinant in Eq. (31) is complex, a proper branch of the logarithm must be taken in order to make γ_t continuous in time. If continuity were not imposed on γ_t, the wavepacket would show sudden jumps by $\pm\pi$ in the overall phase. Phase continuity is also important in the evaluation of the correlation function (to be discussed in Section V), which requires taking a square root of a complex determinant $\det(A_0 + A_t)$. The continuity of the correlation function is enforced by taking the appropriate branch of the square root.

C. Extended thawed Gaussian approximation (ETGA)

To tackle the propagation of more general initial states, Lee and Heller (1982) proposed an extension of the TGA that assumes the initial state to be a Gaussian multiplied by a polynomial (Lee and Heller, 1982; Patoz et al., 2018):

$$\phi(q,0) = P\left(q - q_0\right)\psi(q,0). \tag{32}$$

The basic idea of the *extended TGA* (ETGA) is the same as of the original TGA; it uses the local harmonic approximation (17) for the potential along the trajectory q_t, but makes no other approximation.

Because the only dependence of $\psi(q,0)$ on p_0 comes from the exponent $p_0^T \cdot (q - q_0)$ [see Eq. (15)], the polynomial prefactor in Eq. (32) can be replaced by the *same* polynomial in the derivatives with respect to p_0:

$$\phi(q,0) = P\left(\frac{\hbar}{\mathrm{i}}\frac{\partial}{\partial p_0}\right)\psi(q,0). \tag{33}$$

Appendix D of Begušić et al. (2018a) provides a detailed proof that the local harmonic approximation implies that the ETGA wavepacket at time t has the simple form (Lee and Heller, 1982)

$$\phi(q,t) = P\left(\frac{\hbar}{\mathrm{i}}\frac{\partial}{\partial p_0}\right)\psi(q,t), \tag{34}$$

where the dependence of $\psi(q,t)$ on initial conditions q_0 and p_0 is taken into account. In particular, equations of motion (18)-(21) for q_t, p_t, A_t, and γ_t remain unchanged.

As for the parameters of the polynomial, the simplest possibility beyond the original TGA is to consider only the constant and linear terms, which will be the only ones required in the Herzberg–Teller approximation (66) for the transition dipole moment, used in Subsection V D for calculations of electronic spectra beyond the Condon approximation. Appendix D of Begušić et al. (2018a) provides a detailed demonstration that in this case (Lee and Heller, 1982)

$$\phi(q,t) = \left[a_0 + b_t^T \cdot (q - q_t)\right]\psi(q,t), \tag{35}$$

where the linear parameter of the polynomial at time t is

$$b_t = (-A_t \cdot M_{t,qp} + M_{t,pp}) \cdot b_0 \tag{36}$$

$$= (Q_0 \cdot Q_t^{-1})^T \cdot b_0. \tag{37}$$

Because all ingredients needed in Eq. (36) are already evaluated for the propagation of the parameters of the Gaussian, the evaluation of b_t comes at almost no additional cost.

D. Multiple thawed Gaussians (n-TGA)

Another natural way to generalize the TGA is by considering superpositions

$$\psi(q,t) = \sum_{i=1}^{n} c_i \psi_i(q,t), \tag{38}$$

of thawed Gaussian wavepackets $\psi_i(q,t)$, where each component $\psi_i(q,t)$ is normalized at time 0 and propagated with its own effective time-dependent Hamiltonian $\hat{H}_{\mathrm{eff},i}(t)$ according to the original TGA prescription. Let us call this method *multiple thawed Gaussians* or *n-TGA*. The expansion (38) is useful only if the initial state $\psi(q,0)$ is accurately represented by a small number of Gaussians; below, we shall see an example with $n = 3$. If n is very large, it is more convenient to use the frozen Gaussians (Heller, 1981a), which are easier to propagate.

E. (Non)conservation of norm, inner product, and energy

One of the basic properties of quantum evolution is the conservation of probability, which is reflected in the conservation of the norm of the wavefunction:

$$\|\psi_t\| = \|\hat{U}(t)\psi_0\|, \tag{39}$$

where $\|\psi\|^2 = \langle\psi|\psi\rangle$ and $\hat{U}(t) = \exp(-\mathrm{i}\hat{H}t/\hbar)$ is a time-evolution operator for a time-independent Hermitian Hamiltonian $\hat{H}$. [In Eq. (39), we have and, in the rest of this short section, we shall use a shorthand notation ψ_t for $\psi(t)$.] It is easy to show that time-independent Hamiltonians conserve energy, defined as the expectation value

$$E_t := \langle\psi_t|\hat{H}|\psi_t\rangle \tag{40}$$

of the Hamiltonian:

$$E_t := \langle\psi_0|\hat{U}(t)^\dagger\hat{H}\hat{U}(t)|\psi_0\rangle = \langle\psi_0|\hat{U}(t)^\dagger\hat{U}(t)\hat{H}|\psi_0\rangle = \langle\psi_0|\hat{H}|\psi_0\rangle = E_0, \tag{41}$$

where we used the facts that $\hat{U}(t)$ commutes with $\hat{H}$ and that $\hat{U}$ is unitary, i.e.,

$$\hat{U}^\dagger\hat{U} = [\exp(-\mathrm{i}\hat{H}t/\hbar)]^\dagger\exp(-\mathrm{i}\hat{H}t/\hbar) = \hat{U}^{-1}\hat{U} = 1 \tag{42}$$

because $\hat{H}$ is Hermitian. The conservation of norm remains valid even for time-dependent Hermitian Hamiltonians $\hat{H}(t)$, for which the time-evolution operator is a function of both the initial and final times:

$$\hat{U}(t,t_0) = \mathcal{T}\exp\left(-\mathrm{i}\int_{t_0}^{t}\hat{H}(\tau)\mathrm{d}\tau/\hbar\right). \tag{43}$$

In contrast, the energy is not conserved because $[\hat{H}(t),\hat{U}(t,t_0)] \neq 0$ since even $[\hat{H}(t_1),\hat{H}(t_2)] \neq 0$ in general for two different times t_1 and t_2.

It is easy to show that if the evolution operator $\hat{U}(t,t_0)$ conserves not only the norm, but also the inner product $\langle\psi_t|\phi_t\rangle$, then $\hat{U}(t,t_0)$ must be linear. Conservation of the inner product implies, of course, the conservation of the norm, since $\|\psi\| = \langle\psi|\psi\rangle^{1/2}$. However, there are operators $\hat{U}(t,t_0)$ that conserve the norm but not the inner product; by the previous argument such operators must be nonlinear.

The time-evolution operator of the TGA is a perfect example of such a "pathological" operator because it corresponds to a time-dependent effective Hamiltonian $\hat{H}_{\mathrm{eff}}(t)$ that depends on the initial state ψ_0. Therefore

$$\hat{U}_{\mathrm{TGA}} \equiv \hat{U}_{\mathrm{TGA}}(t,t_0,\psi_0), \tag{44}$$

which implies that it is a nonlinear operator. It comes as no surprise that $\hat{U}_{\mathrm{TGA}}$ does not preserve the inner product between two different states:

$$\langle\psi_t|\phi_t\rangle = \langle\psi_0|\hat{U}_{\mathrm{TGA}}(t,t_0,\psi_0)^\dagger\hat{U}_{\mathrm{TGA}}(t,t_0,\phi_0)|\phi_0\rangle \neq \langle\psi_0|\phi_0\rangle\,. \tag{45}$$

In contrast, $\hat{U}_{\mathrm{TGA}}$ still conserves the norm of any initial state:

$$\begin{aligned}\|\psi_t\|^2 &= \langle\psi_t|\psi_t\rangle = \langle\psi_0|\hat{U}_{\mathrm{TGA}}(t,t_0,\psi_0)^\dagger \hat{U}_{\mathrm{TGA}}(t,t_0,\psi_0)|\psi_0\rangle \\ &= \langle\psi_0|\psi_0\rangle = \|\psi_0\|^2 .\end{aligned}$$

Finally, the non-conservation of energy by the TGA follows from the time dependence of $\hat{H}_{\mathrm{eff}}(t)$. In fact, one can go further and partition the energy of the thawed Gaussian wavepacket as $E_{\mathrm{TGA}} = E_{\mathrm{cl}} + E_{\mathrm{sc}}$ into a "classical" energy of the guiding trajectory,

$$E_{\mathrm{cl}} = H(q_t,p_t) = \frac{1}{2} p_t^T \cdot m^{-1} \cdot p_t + V(q_t), \tag{46}$$

and the "semiclassical" energy associated with the finite width of the wavepacket:

$$\begin{aligned} E_{\mathrm{sc}} &= \frac{1}{2}\,\mathrm{Tr}\left(m^{-1}\cdot\Pi_t^2\right) + \frac{1}{2}\,\mathrm{Tr}\left(\mathrm{Hess}_q\, V|_{q_t}\cdot\Sigma_t^2\right) && (47)\\ &= H_{\mathrm{sc}}(Q_t,P_t;q_t), && (48)\end{aligned}$$

where

$$\Sigma_t^2 := \langle\psi_t|(\hat{q}-q_t)\otimes(\hat{q}-q_t)^T|\psi_t\rangle = \frac{\hbar}{2}(\mathrm{Im}\,A_t)^{-1} = Q_t\cdot Q_t^\dagger, \tag{49}$$

$$\Pi_t^2 := \langle\psi_t|(\hat{p}-p_t)\otimes(\hat{p}-p_t)^T|\psi_t\rangle = \frac{\hbar}{2} A_t\cdot(\mathrm{Im}\,A_t)^{-1}\cdot A_t^\dagger = P_t\cdot P_t^\dagger \tag{50}$$

are position and momentum width (covariance) matrices. Since the guiding trajectory (q_t,p_t) is propagated with the exact, time-independent Hamiltonian $H(q,p)$, the classical energy E_{cl} is conserved exactly. In contrast, the semiclassical contribution $E_{\mathrm{sc}} = H_{\mathrm{sc}}(Q_t,P_t;q_t)$ can be interpreted as a classical energy of the trajectory (Q_t,P_t) guided by a Hamiltonian $H_{\mathrm{sc}}(Q,P;q_t)$ that depends on time via q_t. As a result, E_{sc} depends on time and is responsible for the nonconservation of the total energy E_{TGA}.

From Eqs. (46) and (48), it follows that the total energy can be written as

$$E_{\mathrm{TGA}} = H(q_t,p_t) + H_{\mathrm{sc}}(Q_t,P_t;q_t) \tag{51}$$

Although it may be tempting, the sum in the right-hand side of Eq. (51) cannot be interpreted as a classical Hamiltonian in variables q, p, Q, and P; whereas the equations (18), (25), and (26) for $\dot{q}_t$, $\dot{Q}_t$, and $\dot{P}_t$ can, indeed, be obtained as Hamilton's equations of motion for such a "total Hamiltonian", the classical equation of motion for p_t [Eq. (19)] does not contain a term arising from the dependence of H_{sc} on q_t. Interestingly, if the dependence of H_{sc} on q_t vanishes, which happens in a global harmonic potential or if one approximates $\mathrm{Hess}_q\, V|_{q_t}$ at all times by a constant, reference Hessian, the right-hand side of Eq. (51) *can* be interpreted as a Hamiltonian $H(q,p,Q,P)$, and the energy is conserved exactly (Begušić et al., 2019).

The above considerations generalize easily to the ETGA. The corresponding evolution operator $\hat{U}_{\mathrm{ETGA}}$ again depends on both the initial and final time as well as on the initial state ϕ_0. Expression (34) for $\phi(q,t)$ implies that $\hat{U}_{\mathrm{ETGA}}$ is fully determined by these three parameters, so

$$\hat{U}_{\mathrm{ETGA}} \equiv \hat{U}_{\mathrm{ETGA}}(t, t_0, \phi_0). \tag{52}$$

As a consequence, the ETGA conserves the norm, but both the inner product and energy generally depend on time.

By now it should be obvious that multiple thawed Gaussians do not even preserve the norm of the initial state. It is a simple consequence of the nonconservation of the inner product by the TGA:

$$\|\psi_t\|^2 = \sum_{i,j=1}^{n} c_i^* c_j \langle \psi_{i,t} | \psi_{j,t} \rangle \neq \sum_{i,j=1}^{n} c_i^* c_j \langle \psi_{i,0} | \psi_{j,0} \rangle = \|\psi_0\|^2 . \tag{53}$$

Because they do not conserve the norm, the multiple thawed Gaussians do not conserve the inner product either. That the energy generally depends on time is clear.

V. TIME-DEPENDENT APPROACH TO ELECTRONIC SPECTROSCOPY

Quantum and semiclassical dynamics methods, discussed in Sections III and IV, yield the quantum or semiclassical molecular wavepacket at time t. In order to compare with experimental electronic spectra, it is necessary to translate the knowledge of the time-dependent molecular state to a cross-section that can be measured experimentally. To be specific, let us inspect in detail the linear electronic absorption spectrum and, at the end, mention briefly the main differences that show up in nonlinear spectroscopy on the example of time-resolved stimulated emission spectrum.

A. Linear absorption spectra

Within the *electric-dipole approximation* and first-order *time-dependent perturbation theory*, the absorption cross section for a linearly polarized light of frequency ω can be expressed as the Fourier transform

$$\sigma(\vec{\epsilon}, \omega) \approx \frac{\omega}{2\hbar c \varepsilon_0} \int_{-\infty}^{\infty} C_{\mu\mu}(\vec{\epsilon}, t) e^{\mathrm{i}\omega t} \mathrm{d}t \tag{54}$$

of the dipole time autocorrelation function

$$C_{\mu\mu}(\vec{\epsilon}, t) = \mathrm{Tr}\left[\hat{\boldsymbol{\rho}} \hat{\boldsymbol{\mu}}(t) \hat{\boldsymbol{\mu}}\right], \tag{55}$$

where $\vec{\epsilon}$ is the unit polarization vector of the electric field, $\hat{\boldsymbol{\rho}}$ is the density operator of the initial state, $\hat{\boldsymbol{\mu}} := \vec{\epsilon} \cdot \hat{\vec{\boldsymbol{\mu}}}$ is the projection of the molecular electric dipole operator on the direction $\vec{\epsilon}$ of the field, and

$$\hat{\boldsymbol{\mu}}(t) = e^{\mathrm{i}\hat{\boldsymbol{H}}t/\hbar}\hat{\boldsymbol{\mu}}e^{-\mathrm{i}\hat{\boldsymbol{H}}t/\hbar} \tag{56}$$

is this projected molecular dipole moment operator at time t (in the Heisenberg picture). Assuming the *zero temperature approximation*, the initial state is $\hat{\boldsymbol{\rho}} = |1, g\rangle\langle 1, g|$, i.e., the ground vibrational state g of the ground electronic state 1; in particular, it is a pure state. Assuming, furthermore, that the incident radiation is in resonance only with a single pair of electronic states 1 and 2 (*quasi-resonance condition*), that those states are not vibronically coupled (*Born-Oppenheimer approximation*), the dipole time autocorrelation function reduces (Heller, 1981b) to

$$C_{\mu\mu}(\vec{\epsilon}, t) \approx \langle 1, g|e^{\mathrm{i}\hat{H}_1 t/\hbar}\hat{\mu}_{12}e^{-\mathrm{i}\hat{H}_2 t/\hbar}\hat{\mu}_{21}|1, g\rangle \tag{57}$$

where $\hat{H}_1$ and $\hat{H}_2$ are the nuclear Hamiltonian operators in the ground and excited electronic states, and $\hat{\mu}_{21}$ is the matrix element of the projected molecular transition dipole moment matrix $\hat{\boldsymbol{\mu}}$.

To evaluate the autocorrelation function (57), let us rewrite it, without any further approximation, as

$$C_{\mu\mu}(\vec{\epsilon}, t) \approx C_{\phi\phi}(t)e^{\mathrm{i}E_{1,g}t/\hbar} \tag{58}$$

in terms of the vibrational zero-point energy $E_{1,g}$ of the ground electronic state and wavepacket autocorrelation function

$$C_{\phi\phi}(t) = \langle\phi(0)|\phi(t)\rangle \tag{59}$$

of the (un-normalized) initial wavepacket $|\phi(0)\rangle = \hat{\mu}_{21}|1, g\rangle$ propagated on the excited-state surface with the Hamiltonian $\hat{H}_2$:

$$|\phi(t)\rangle = e^{-\mathrm{i}\hat{H}_2 t/\hbar}|\phi(0)\rangle. \tag{60}$$

B. Condon approximation

The electric transition dipole moment is, in general, a function of nuclear coordinates, yet, within the *Condon approximation* (Condon, 1926), this moment is assumed to be independent of the molecular geometry and is commonly approximated with its value at the equilibrium geometry q_{eq} of the initial state:

$$\mu_{12}(q) \approx \mathrm{const} = \mu_{12}(q_{\mathrm{eq}}). \tag{61}$$

Within the Condon approximation, the spectrum can be written as the Fourier transform

$$\sigma(\vec{\epsilon},\omega) \approx \frac{\omega}{2\hbar c\varepsilon_0}\mu_{12}^2 \int_{-\infty}^{\infty} C_{\psi\psi}(t) e^{\mathrm{i}(\omega+E_{1,g}/\hbar)t}\mathrm{d}t \tag{62}$$

of the wavepacket autocorrelation function

$$C_{\psi\psi}(t) = \langle\psi|\psi(t)\rangle = \langle\psi|e^{-\mathrm{i}\hat{H}_2 t/\hbar}|\psi\rangle \tag{63}$$

of a normalized initial state $|\psi\rangle = |1,g\rangle$.

The beauty of Eqs. (62) and (63) lies in their simple interpretation [see also Fig. 1, left]: the absorption of a photon of frequency ω lifts the stationary vibrational ground state $|\psi\rangle = |1,g\rangle$ of the ground-state surface instantaneously to the excited-state surface, where this, now nonstationary state starts moving under the influence of the excited-state Hamiltonian *alone*. In particular, the explicit form of the electromagnetic field does not play any role and the linear absorption spectrum is determined solely by the field-free dynamics of the wavepacket $\psi(t)$ on the excited-state surface. Indeed, this fact is the essence of *linear response theory*, which is here equivalent to the first order time-dependent perturbation theory.

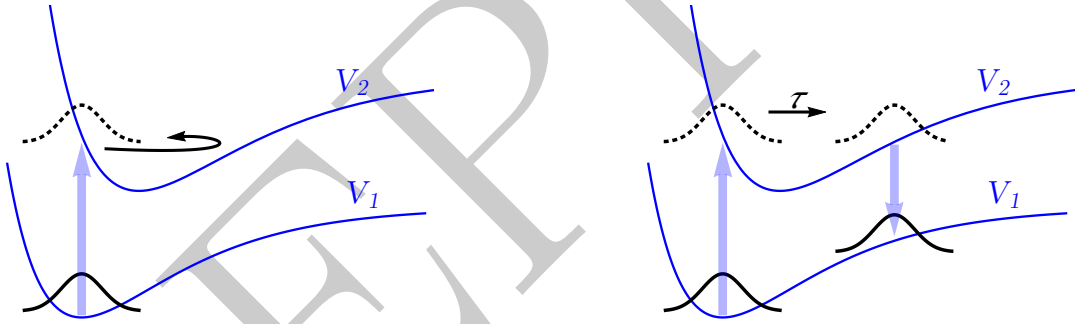

FIG. 1. Schematic representation of physical processes underlying two types of vibrationally resolved electronic spectra. Left: Linear absorption. Right: Time-resolved stimulated emission.

C. Connection to fidelity amplitude

Note that since the initial state $|\psi\rangle \equiv |1,g\rangle$ is an eigenstate of $\hat{H}_1$, the spectrum can be also written as

$$\sigma(\vec{\epsilon},\omega) = \frac{\omega}{\hbar c\varepsilon_0}\mu_{12}^2 \,\mathrm{Re}\int_0^{\infty} f(t) e^{\mathrm{i}\omega t}\mathrm{d}t, \tag{64}$$

where

$$f(t) = \langle\psi_1(t)|\psi_2(t)\rangle = \langle\psi|e^{\mathrm{i}\hat{H}_1 t/\hbar}e^{-\mathrm{i}\hat{H}_2 t/\hbar}|\psi\rangle \tag{65}$$

is a wavepacket cross-correlation function, also known as the *fidelity amplitude* (Gorin et al., 2006), between two states $\psi_1(t)$ and $\psi_2(t)$, both starting from the same initial state ψ, but

one evolved with $\hat{H}_1$ and the other with $\hat{H}_2$. As the name suggests, the fidelity amplitude measures the similarity between the quantum evolutions on the ground and excited surfaces. Not only is expression (64) "nicer" than Eq. (62) because it does not contain the zero-point energy in the exponent, it is also much more general because it remains valid for nonstationary initial states, such as arbitrary superpositions of vibrational eigenstates or states prepared by the pump pulse in time-resolved spectroscopy. Moreover, this alternative, although less known expression for an electronic spectrum is not just a mathematical curiosity; indeed, it is the direct outcome of the derivation of the spectrum using the first-order time-dependent perturbation theory, and it is only due to the *additional* assumption that ψ is a vibrational ground state (or another eigenstate) of $\hat{H}_1$ that one obtains the much better known expression (62) for the spectrum in terms of the wavepacket autocorrelation function (63).

The more general correlation function (65) has many important applications: Outside of electronic spectroscopy (Egorov et al., 1998, 1999; Li et al., 1996; Pollard et al., 1990b; Rost, 1995; Shemetulskis and Loring, 1992; Shi and Geva, 2005), it has proved useful, e.g., in NMR spin echo experiments (Pastawski et al., 2000) and theories of quantum computation (Gorin et al., 2006), decoherence (Gorin et al., 2006), and inelastic neutron scattering (Petitjean et al., 2007). In chemical physics, the fidelity amplitude was also used as a measure of the dynamical importance of diabatic (Zimmermann and Vaníček, 2010), nonadiabatic (Zimmermann and Vaníček, 2012a), or spin-orbit couplings (Zimmermann and Vaníček, 2012b), and of the accuracy of molecular quantum dynamics on an approximate potential energy surface (Li et al., 2009; Zimmermann et al., 2010).

D. Herzberg-Teller approximation

The widespread use of the Condon approximation (61) is justified by its validity in many systems; it can describe most of the strongly symmetry-allowed transitions both qualitatively and quantitatively. However, a number of molecules exhibit "electronically forbidden" transitions, i.e., transitions $\alpha \leftarrow \beta$ with $\vec{\mu}_{\alpha\beta}(q_{\mathrm{eq}}) = 0$, which cannot be described within the Condon approximation. Such systems, as well as systems in which the Condon term is small but not exactly zero, can be treated with the *Herzberg–Teller approximation* (Herzberg and Teller, 1933) that takes into account at least the gradient of the transition dipole moment with respect to nuclear degrees of freedom:

$$\vec{\boldsymbol{\mu}}(q) \approx \vec{\boldsymbol{\mu}}(q_{\mathrm{eq}}) + \partial_q \vec{\boldsymbol{\mu}}|^T_{q_{\mathrm{eq}}} \cdot (q - q_{\mathrm{eq}}). \tag{66}$$

Although the Herzberg–Teller approximation is often discussed in terms of vibronic couplings between different electronic states (Seidner et al., 1992), this relation is not obvious from Eq. (66). It becomes, however, clear from a remarkable equality (Begušić et al., 2018a;

Patoz et al., 2018)

$$\partial_{q_j}\vec{\boldsymbol{\mu}}(q) = [\vec{\boldsymbol{\mu}}(q), \boldsymbol{F}_j(q)] + \partial_{q_j}\vec{\mu}_{\mathrm{nu}}(q)\mathbf{1} \tag{67}$$

satisfied by the gradient of the matrix representation $\vec{\boldsymbol{\mu}}(q)$ of the molecular dipole operator $\hat{\vec{\mu}}_{\mathrm{mol}}$ at the nuclear configuration q. In this equation, matrix elements of $\vec{\boldsymbol{\mu}}(q)$ are defined as partial, electronic expectation values

$$\vec{\mu}_{\alpha\beta}(q) := \langle\alpha(q)|\hat{\vec{\mu}}_{\mathrm{mol}}|\beta(q)\rangle, \tag{68}$$

elements of the matrix $\boldsymbol{F}_j(q)$ of nonadiabatic vector couplings are obtained as

$$F_{\alpha\beta,j} := \langle\alpha(q)|\partial_{q_j}\beta(q)\rangle, \tag{69}$$

and $\vec{\mu}_{\mathrm{nu}}$ is the nuclear component of $\hat{\vec{\mu}}_{\mathrm{mol}}$.

Direct interpretation of relation (67), which is proven in Appendix B of Begušić et al. (2018a), explains the concepts of *vibronic transitions* and *intensity borrowing*. Namely, the gradient of the transition dipole moment between states α and β can be nonzero only if there exists an intermediate state γ that is nonadiabatically (i.e., *vibronically*) coupled to one of the states and electric-dipole coupled to the other state. Typically, the nonadiabatic couplings with the ground state ($\beta = 1$) can be neglected at the ground-state optimized geometry, around which the transition dipole moment is expanded. This leads to an expression (Li et al., 2010)

$$\partial_{q_j}\vec{\mu}_{\alpha 1} \approx -\sum_{\gamma} F_{\alpha\gamma,j}\vec{\mu}_{\gamma 1} \tag{70}$$

that explains the meaning of *intensity borrowing*, in which the symmetry forbidden transition to the formally dark state α occurs due to borrowing of the transition intensity from the neighboring bright electronic states γ that are vibronically coupled to the state α. Note that, despite introducing nonadiabatic couplings between excited electronic states, the original Born-Oppenheimer picture may be valid—the vibronic couplings that induce the transition do not necessarily influence the nuclear wavepacket dynamics. Although these nonadiabatic couplings are essential for describing the existence of symmetry-forbidden spectra, their contribution to the field-free Hamiltonian of the system may be negligible. The rather high resolution of the absorption spectrum of benzene (discussed in Section VIII B) supports these considerations—otherwise, significant population transfer would lead to the shortening of the excited-state lifetime and, consequently, to significant broadening of the spectral lines.

E. Rotational averaging of the spectrum

To compare with an experiment in gas phase or another isotropic medium, one has to average the vibronic spectrum (54) over all orientations of the molecule with respect to the

polarization $\vec{\epsilon}$ of the electric field. This procedure assumes the rotations to be classical and, therefore, cannot be used to compute rotationally resolved spectra.

Within the Condon approximation, the transition dipole moment is independent of coordinates, and this averaging is trivial, namely

$$\overline{C_{\mu\mu}(\vec{\epsilon}, t)} = \frac{1}{3} C_{|\vec{\mu}||\vec{\mu}|}(t), \tag{71}$$

where $|\vec{\mu}|$ is the magnitude of the transition dipole moment, so only a single calculation is required—for the transition dipole moment aligned with the field.

For a general dipole moment (Andrews and Thirunamachandran, 1977; Gelin et al., 2017), it is useful to define the spectrum *tensor* $\overleftrightarrow{\sigma}(\omega)$, from which the spectrum (54) for a specific polarization $\vec{\epsilon}$, is obtained by "evaluation":

$$\sigma(\vec{\epsilon}, \omega) = \vec{\epsilon}^T \cdot \overleftrightarrow{\sigma}(\omega) \cdot \vec{\epsilon}. \tag{72}$$

The *rotational averaging* of the spectrum corresponds to the averaging of $\sigma(\vec{\epsilon}, \omega)$ over all unit vectors $\vec{\epsilon}$. Due to the isotropy of the 3-dimensional Euclidean space, the average over all orientations need not be performed numerically, and is, instead, reduced to an arithmetic average over only three arbitrary orthogonal orientations of the molecule with respect to the field:

$$\begin{aligned} \overline{\sigma(\vec{\epsilon}, \omega)} &= \frac{1}{3} \operatorname{Tr} \overleftrightarrow{\sigma}(\omega) \\ &= \frac{1}{3} \left[\sigma_{xx}(\omega) + \sigma_{yy}(\omega) + \sigma_{zz}(\omega)\right] \\ &= \frac{1}{3} \left[\sigma(\vec{e}_x, \omega) + \sigma(\vec{e}_y, \omega) + \sigma(\vec{e}_z, \omega)\right]. \end{aligned} \tag{73}$$

Appendix A of Begušić et al. (2018a) contains an explicit proof of these equalities. Within the Condon approximation, in which $\vec{\mu}$ is coordinate-independent, the orientational average (73) simplifies further into the standard textbook recipe (71).

F. Time-resolved electronic spectra

In the case of nonlinear spectra, the autocorrelation picture is no longer valid. In contrast, the more general picture using fidelity amplitude (64) still applies. A wide variety of nonlinear time-resolved spectra belong to the pump-probe scheme, in which an ultrashort pump pulse prepares a nonstationary nuclear wavepacket in an excited electronic state, and an ultrashort probe pulse measures the dynamics of this wavepacket after a certain time delay τ. There are many possible experimental setups depending on the polarization and mutual orientation of the pump and probe laser beams and on the direction in which the signal is detected (Mukamel, 1999), but, to be specific, we will only consider time-resolved stimulated emission here [see Fig. 1, right].

Besides the assumptions used for linear spectra, a simplified picture of time-resolved stimulated emission assumes that the pump and probe pulses can be treated independently (*nonoverlapping pulses approximation*) and are short compared with the nuclear vibrational period and, at the same time, long compared with the time scale of the relevant electronic transition (*ultrashort pulse approximation*).

Assuming the validity of the zero-temperature, electric dipole, rotating-wave, and Condon approximations, and combining them with the third-order time-dependent perturbation theory, one obtains the differential time-resolved stimulated emission spectrum at frequency ω and time delay τ between the pump and probe pulses as the Fourier transform

$$\sigma(\omega, \tau) \propto \mathrm{Re} \int_0^\infty \mathrm{d}t \, f(t,\tau) \, e^{\mathrm{i}\omega t} \tag{74}$$

of the wavepacket correlation function (Pollard et al., 1990b; Šulc and Vaníček, 2012; Wehrle et al., 2011)

$$f(t, \tau) = \langle \psi_1(t, \tau) | \psi_2(t, \tau) \rangle, \tag{75}$$

where τ is the time delay between the pump and probe pulses, t denotes the time elapsed after the probe pulse, and

$$|\psi_\alpha(t, \tau)\rangle := e^{-\mathrm{i}\hat{H}_\alpha t/\hbar} e^{-\mathrm{i}\hat{H}_2 \tau/\hbar} |\psi\rangle \tag{76}$$

stands for the initial state evolved for the delay time τ with the excited state Hamiltonian and subsequently for time t with either the ground or excited state Hamiltonian ($\alpha = 1, 2$).

As written, the correlation function $f(t,\tau)$ from Eq. (75) has an immediate interpretation as the quantum fidelity amplitude between states $\psi_1(t, \tau)$ and $\psi_2(t, \tau)$. This fidelity amplitude now corresponds to evolutions for time $t + \tau$ of the same initial state ψ with two Hamiltonians, a time-independent Hamiltonian equal to $\hat{H}_2$ and a time-dependent Hamiltonian equal to $\hat{H}_2$ until time τ, and equal to $\hat{H}_1$ at later times. Note that the correlation function $f(t,\tau)$ can be also interpreted as a correlation function (65) from linear spectroscopy, but applied to a nonstationary initial state $\exp(-\mathrm{i}\tau\hat{H}_2/\hbar)|\psi\rangle$ prepared by the pump pulse (Pollard et al., 1990b; Shemetulskis and Loring, 1992).

VI. "STANDARD MODELS" OF ELECTRONIC SPECTROSCOPY

Having reviewed the time-dependent approach to spectroscopy, we are ready to discuss several models commonly used for approximating molecular potential energy surfaces in calculations of vibrationally resolved electronic spectra. Due to their simplicity, these models facilitate approximate evaluations of spectra even of molecules for which obtaining more accurate surfaces would be impossible. Moreover, it is easier to analyze these models than the exact potential surfaces.

From now on, we assume that translations have been removed and that rovibrational coupling can be neglected within the accuracy provided by the methods used for dynamics. Therefore, we may assume that the nuclear Hamiltonian for the αth electronic state of a nonlinear polyatomic molecule has been reduced from $3N$ to $D = 3N - 6$ dimensions, and is expressed in normal mode coordinates as

$$H_\alpha(q,p) = \frac{1}{2} p^T \cdot m^{-1} \cdot p + V_\alpha(q), \tag{77}$$

where q and p are D-dimensional vectors of position and momentum, and m is a D-dimensional diagonal mass matrix.

In *vibrational spectroscopy*, only one electronic state is involved, and therefore only one potential energy surface is needed. The simplest model is the harmonic potential,

$$V_1(q) = \frac{1}{2}(q - q_1)^T \cdot k_1 \cdot (q - q_1), \tag{78}$$

where k_1 is a D-dimensional diagonal force constant matrix and where we assume that the minimum occurs at $q = q_1$ with energy $V_1(q_1) = 0$. The harmonic model often provides a good approximation close to the minimum of a potential energy surface, but breaks down, of course, in anharmonic and floppy systems.

In *electronic spectroscopy*, the situation is much richer because energy surfaces describing different electronic states can have different minima, different force constants, and even different normal modes. To be specific, let us consider only two electronic states. The simplest model for the excited state surface is the *displaced harmonic potential*

$$V_2(q) := \Delta E + V_1(q - \Delta q) = \Delta E + \frac{1}{2}\left(q - q_2\right)^T \cdot k_1 \cdot \left(q - q_2\right), \tag{79}$$

where ΔE is the adiabatic excitation energy and $\Delta q = q_2 - q_1$ is the displacement from the minimum of the harmonic potential V_1 given by Eq. (78). Modes j with nonzero Δq_j are the modes *excited* by the electronic transition.

There are two natural ways to construct displaced harmonic models as approximations to an anharmonic system: the adiabatic shift and vertical gradient approximations. Both methods use Eqs. (78) and (79) with k_1 given by the Hessian of the ground surface at the equilibrium geometry, and thus avoid computing excited-state Hessians. In the *adiabatic shift approximation*, q_2 is given by the optimized excited-state geometry, whereas in the *vertical gradient approximation*, this optimization is avoided and the q_2 parameter in the model (79) is obtained by evaluating the gradient of the *ab initio* excited-state potential energy at the ground-state equilibrium geometry (Avila Ferrer and Santoro, 2012; Egidi et al., 2014; Fortino et al., 2019):

$$q_2 := q_1 - k_1^{-1} \cdot \mathrm{grad}_q \, V_{2,\text{ab initio}}|_{q_1}. \tag{80}$$

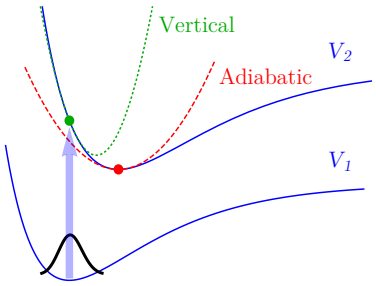

FIG. 2. In the vertical harmonic and adiabatic harmonic models, the excited-state potential energy is expanded to the second order about the minimum of the ground-state and excited-state potential energy surfaces, respectively.

An improvement that accounts for changes in the force constants in the excited state is provided by the *displaced and distorted harmonic potential*

$$V_2(q) := \Delta E + \frac{1}{2}(q - q_2)^T \cdot k_2 \cdot (q - q_2) \tag{81}$$

with a diagonal matrix $k_2 \neq k_1$. Finally, one can also include the *Duschinsky rotation* between the ground-state and excited-state normal modes, to obtain the most general *harmonic model*, described still by Eq. (81), but allowing a general $D \times D$ symmetric force constant matrix k_2.

A harmonic model, given by Eqs. (78) and (81), which has been constructed as an approximation to an anharmonic system, is said to be a global *harmonic approximation*. Among all possible global harmonic approximations, two special ones stand out. In the *vertical harmonic approximation*, both V_1 and V_2 are expanded to the second order about the minimum of the ground state potential V_1 (see Fig. 2). This approach provides a good approximation in the Franck-Condon region, and is therefore expected to be accurate for short propagation times, which determine the initial decay of the autocorrelation function $C(t)$ and hence the overall envelope of the electronic spectrum. In the *adiabatic harmonic approximation*, in contrast, each V_α is expanded about its own minimum (see Fig. 2); in particular, k_2 is given by the Hessian of V_2 at the minimum of V_2. Often, but not always, this second approach provides a better approximation for the period of oscillations and hence for the vibrational peak spacing in the spectra.

Further improvements require including anharmonicity. The one-dimensional *Morse potential*

$$V_\alpha(q) = V_{\alpha,0} + d_\alpha(1 - e^{-a_\alpha(q-q_\alpha)})^2 \tag{82}$$

is a good starting point for including anharmonicity of the degrees of freedom corresponding to bond stretches. In Eq. (82), q_α is again the location of the minimum $V_{\alpha,0}$ of the potential, while parameters a_α and d_α are both related to the curvature and anharmonicity of the potential. The adiabatic excitation energy is given by the difference $\Delta E := V_{2,0} - V_{1,0}$.

Anharmonicity in the symmetric torsional or umbrella motions can be represented by a *quartic* perturbation to the quadratic potential:

$$V_\alpha(q) = V_{\alpha,0} + \frac{1}{2}k_\alpha(q-q_\alpha)^2 + \frac{1}{12}\delta_\alpha(q-q_\alpha)^4. \tag{83}$$

Here, δ_α controls the magnitude of the perturbation, and we have, for simplicity, written out V_α explicitly only for one degree of freedom.

One can, of course, generate more accurate anharmonic potential energy surfaces by fitting more sophisticated analytical functions to *ab initio* energies evaluated at an appropriately chosen set of molecular configurations. In contrast, in the *on-the-fly approach*, the potential required for the dynamics is evaluated only along the trajectory; the fitting and construction of global surfaces are avoided. The on-the-fly approach has the advantage that the true molecular potential does not have to be approximated—instead, one can employ the best available electronic structure to obtain the energy at the point of interest. The drawback is, of course, that the on-the-fly approach works only in connection with semiclassical, mixed quantum-classical, or trajectory-based quantum methods, but not with methods that rely on global or semiglobal surfaces.

Finally, in electronic spectroscopy, one can choose to approximate one surface by a global harmonic model, while treating the other with the on-the-fly approach. This *combined global harmonic/on-the-fly approximation* is popular in linear spectroscopy, where the initial wavepacket is commonly the ground vibrational state of the initial electronic state. Because the harmonic approximation is valid near the minimum of the surface, it produces an accurate initial wavepacket. For wavepackets generated this way, the on-the-fly and combined methods are equivalent in the linear spectra calculations. In contrast, in the simulations of time-resolved spectra, the nuclear dynamics is performed in both electronic states; as a result, the global harmonic, combined, and on-the-fly approaches all give different results (Begušić et al., 2018b).

A. Several few-dimensional examples

Let us demonstrate the basic features and shortcomings of various models by computing linear absorption spectra of several few-dimensional examples. The first system is a pair of two-dimensional harmonic potentials with a nondiagonal excited-state force constant, and thus exhibiting the Duschinsky effect. Figure 3 shows the spectra computed using either the global harmonic model, which is exact here, or one of two approximate models. The simpler, displaced harmonic oscillator model does not account for the change in the force constant and, therefore, results in incorrect peak positions and intensities. Including the distortion of the surface in the displaced and distorted harmonic model fixes the peak positions; however,

the intensities are still rather poor because this model neglects the mode-mixing present in the system.

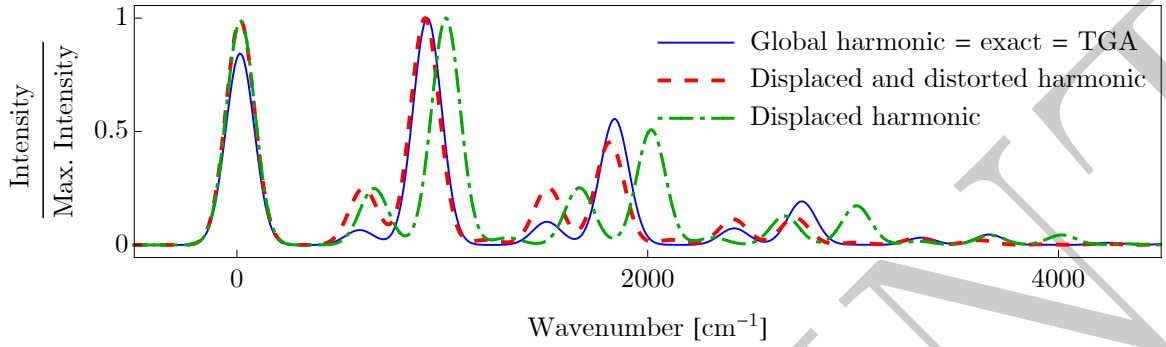

FIG. 3. Absorption spectrum of a pair of two-dimensional harmonic potentials. The excited-state surface is displaced, distorted, and rotated with respect to the ground-state surface. The relative dimensionless displacements $\Delta_i = \sqrt{m_i\omega_{1,i}/2\hbar}(q_{2,i} - q_{1,i})$ between the minima of the two potentials are $\Delta_a = 1$ and $\Delta_b = 0.5$, the wavenumbers of the two modes are $\tilde{\nu}_{1,a} = 1000$ cm^{-1} and $\tilde{\nu}_{1,b} = 650$ cm^{-1} in the ground state, and $\tilde{\nu}_{2,a} = 800$ cm^{-1} and $\tilde{\nu}_{2,b} = 600$ cm^{-1} in the excited state; the modes are coupled via the off-diagonal elements $k_{2,ab} = k_{2,ba} = k_{1,aa}/10$ of the symmetric force constant matrix of the excited state, where $k_{1,aa}$ is the element of the ground-state force constant corresponding to the mode a.

Due to their simplicity, intuitive interpretation, and acceptable accuracy in many molecular systems, global harmonic models have served as the methods of choice for computing vibronic spectra. However, they tend to fail in floppy molecules and the thawed Gaussian approximation aims to correct this by including the anharmonicity of the potential at least partially. Let us see how this works in practice on two examples of one-dimensional quartic potentials (83) with different degrees of anharmonicity.

In the less anharmonic case (Fig. 4A), the vertical harmonic model yields an incorrect peak spacing due to incorrect description of the classical motion of the wavepacket on the excited-state surface. The peak spacing, directly related to the period between the recurrences of the autocorrelation function, is captured correctly with the adiabatic harmonic model, which approximates the classical dynamics much better. However, the envelope of the spectrum is determined not by the position but by the shape of recurrences. The shape, in turn, depends on the width and phase of the wavepacket in the Franck–Condon region. Because the adiabatic harmonic model is not a good representation of the potential in this region, some of the peak intensities are incorrect. In contrast, the vertical model, constructed from the Franck-Condon data, recovers the envelope of the progression almost perfectly. Nevertheless, in this weakly anharmonic system, the adiabatic harmonic model works, overall, better than the vertical model.

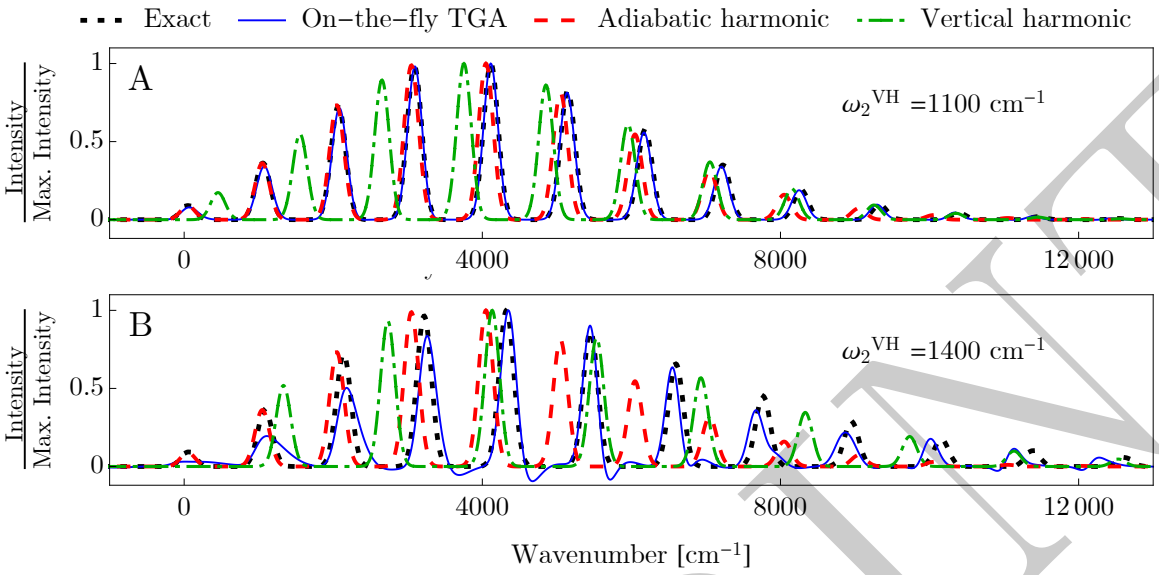

FIG. 4. Absorption spectra of two quartic potentials with different degrees of anharmonicity. In both cases, the ground state is a global harmonic potential of wavenumber $\tilde{\nu}_1 = 1000$ cm^{-1} and the minimum of the excited-state quartic potential is shifted by a relative dimensionless displacement $\Delta = 3$ (see caption of Fig. 3 for definition of Δ). Quartic parameter δ_2 was chosen according to the formula $\delta_2 = (k_2^{\mathrm{VH}} - k_2^{\mathrm{AH}})/(q_{2,i} - q_{1,i})^2$ so that the adiabatic wavenumber was $\tilde{\nu}_2^{\mathrm{AH}} = 800$ cm^{-1} and vertical wavenumber was either (A) $\tilde{\nu}_2^{\mathrm{VH}} = 1100$ cm^{-1} (less anharmonic case) or (B) $\tilde{\nu}_2^{\mathrm{VH}} = 1400$ cm^{-1} (more anharmonic case).

In the more anharmonic case (Fig. 4B), both global harmonic models fail to reproduce the exact spectrum. The adiabatic model no longer recovers the peak spacing and, therefore, describes well only the first few peaks of the progression. The vertical harmonic model again yields incorrect peak positions; however, it performs somewhat better than the adiabatic approach because it reproduces at least the envelope of the spectrum. A similar effect has been observed (Wehrle et al., 2015) in the absorption spectrum of ammonia (see Section VIII below).

Finally, the thawed Gaussian approximation reproduces the exact spectrum better than both global harmonic models because it makes only a local harmonic approximation, which describes the true potential more accurately at all times. In general, modes of different degrees of anharmonicity are excited when a molecule interacts with an external electromagnetic field; however, one cannot know in advance their relative contributions to the spectrum. Therefore, it is hard to decide, *a priori*, whether to use the vertical or adiabatic harmonic model. In contrast, the thawed Gaussian approximation is expected to be at least as accurate as the better of the two global harmonic approaches, and, in addition, requires less human input.

VII. ON-THE-FLY *AB INITIO* IMPLEMENTATION OF THE THAWED GAUSSIAN APPROXIMATION

Because the center of the thawed Gaussian wavepacket follows a classical trajectory, the thawed Gaussian approximation requires only local information about the potential energy surface, and is perfectly suited for on-the-fly evaluation of energies, forces, and Hessians using an *ab initio* electronic structure code. As a consequence, any *ab initio* dynamics code can be easily extended to include the thawed Gaussian approximation.

The computational cost of the Hessian evaluation is often significantly higher than the cost of the corresponding gradients. However, the Hessians of the potential are not needed for the classical propagation of the center of the wavepacket; therefore, Hessians at different points along the classical trajectory can be evaluated in parallel after the full classical trajectory is known, significantly accelerating the calculation. Because the Hessian of the potential energy changes more slowly than its gradient, the computational cost is further reduced by evaluating the Hessians only once in every several steps of the trajectory (typically, every few femtoseconds). The Hessians at intermediate steps can be obtained by interpolation. Alternative approaches exist, such as those based on Hessian updates (Ceotto et al., 2013; Zhuang et al., 2013) or Gaussian process regression (Alborzpour et al., 2016; Laude et al., 2018), in which the frequency of *ab initio* Hessian calculations can be further reduced by using the energies and gradients to improve the accuracy of the interpolation or extrapolation procedure. In summary, if parallelization and interpolation are employed, the Hessian evaluation ceases to be a bottleneck of the thawed Gaussian approximation as it can be often performed even faster than the propagation of a single classical trajectory.

Once all the *ab initio* data are collected, the molecular geometries, gradients, and Hessians of the potential are transformed from the $3N$ Cartesian coordinates to the internal $3N-6$ dimensional coordinate space. The mass-scaled normal mode coordinates are well-suited for vibrational dynamics of molecules: they provide an intuitive interpretation of the dynamics and spectra in terms of the vibrational modes of one electronic state. Although some electronic structure codes accept normal-mode and even general internal coordinates as input, working with the Cartesian coordinates to communicate between the dynamics and electronic structure codes is much more robust.

The coupling between the internal (vibrational) and external (translational and rotational) degrees of freedom is reduced by translating and rotating the molecular configuration to the Eckart frame. Let ξ^{ref} be the $3N$-dimensional Cartesian coordinate vector of a reference configuration and ξ a corresponding vector of a general configuration that we wish to transform. Furthermore, let X_A denote the 3-dimensional vector representing the coordinates of the Ath atom and $X := (X_1, X_2, \ldots, X_N)$ the $3 \times N$ matrix containing the coordinates of all atoms. Finally, let M_A be the mass of the Ath atom and M the $N \times N$

diagonal matrix with N atomic masses on the diagonal.

The translations are separated and the translational Eckart condition,

$$\sum_{A=1}^{N} M_A X_A^{\text{trans}} = 0, \tag{84}$$

is satisfied in the center-of-mass coordinate frame, $X_A^{\text{trans}} := X_A - X_{\text{CM}}$, where

$$X_{\text{CM}} := \sum_{A=1}^{N} M_A X_A / \sum_{A=1}^{N} M_A \tag{85}$$

is the center-of-mass coordinate vector. Satisfying the rotational Eckart condition,

$$\sum_{A=1}^{N} M_A X_A^{\text{ref}} \times X_A^{\text{rot}} = 0, \tag{86}$$

where $X_A^{\text{rot}} := R \cdot X_A^{\text{trans}}$ and R denotes a rotation matrix, is equivalent to finding a 3×3 special orthogonal matrix R that minimizes the square distance

$$\left\| X^{\text{ref}} - X^{\text{rot}} \right\|^2 := \sum_{A=1}^{N} M_A \left| X_A^{\text{ref}} - X_A^{\text{rot}} \right|^2 \tag{87}$$

in the mass-scaled Cartesian coordinates between the reference configuration X^{ref} and the final translated and rotated configuration X^{rot} (Kudin and Dymarsky, 2005); this problem can be solved, e.g., with the Kabsch (Kabsch, 1978) or quaternion (Coutsias et al., 2004; Kearsley, 1989) algorithm. The Kabsch algorithm consists in computing the 3×3 cross-covariance matrix

$$S = X^{\text{trans}} \cdot M \cdot (X^{\text{ref}})^T, \tag{88}$$

finding its singular value decomposition $S = U \Sigma V^T$ (where U and V are real orthogonal matrices), and finally recovering the rotation matrix through

$$R = V \begin{pmatrix} 1 & 0 & 0 \\ 0 & 1 & 0 \\ 0 & 0 & \det(VU^T) \end{pmatrix} U^T. \tag{89}$$

To summarize the procedure of separating translations and rotations in a single equation, let us revert to the $3N$-dimensional vector space notation and define a $3N \times 3N$ block-diagonal rotation matrix R_ξ, composed of N identical 3×3 rotation matrices R on the diagonal, and a $3N$-dimensional center-of-mass configuration ξ_{CM} containing the N three-dimensional vectors X_{CM}. The final rotated and translated configuration is given by

$$\xi^{\text{rot}} = R_\xi \cdot (\xi - \xi_{\text{CM}}). \tag{90}$$

Let O be the orthogonal matrix that diagonalizes the mass-scaled Cartesian Hessian matrix evaluated at ξ^{ref}, i.e.,

$$O^T \cdot m^{-1/2} \cdot \mathrm{Hess}_\xi V|_\xi^{\mathrm{ref}} \cdot m^{-1/2} \cdot O = \Omega^2, \tag{91}$$

where m is the $3N \times 3N$ diagonal mass matrix and Ω a $3N \times 3N$ diagonal matrix with normal mode frequencies on the diagonal. Then, the transformation from Cartesian to mass-scaled normal mode coordinates is given by

$$q = L^T \cdot m^{\frac{1}{2}} \cdot (\xi^{\mathrm{rot}} - \xi^{\mathrm{ref}}), \tag{92}$$

where L is a $3N \times (3N-6)$ submatrix of O from which the six translational and rotational degrees of freedom are dropped. Similarly, the gradients and Hessians are transformed using

$$\mathrm{grad}_q V = L^T \cdot m^{-\frac{1}{2}} \cdot R_\xi \cdot \mathrm{grad}_\xi V, \tag{93}$$

$$\mathrm{Hess}_q V = L^T \cdot m^{-\frac{1}{2}} \cdot R_\xi \cdot \mathrm{Hess}_\xi V \cdot R_\xi^T \cdot m^{-\frac{1}{2}} \cdot L. \tag{94}$$

VIII. EXAMPLES OF ON-THE-FLY *AB INITIO* CALCULATIONS OF ELECTRONIC SPECTRA

Having presented, in Section VI A, simple examples demonstrating merits and shortcomings of commonly used models for describing electronic spectra, let us look at realistic examples based on the on-the-fly *ab initio* calculations of molecules of increasing size. The examples use the thawed Gaussian approximation and its extensions (the extended TGA and the 3TGA), described in Section IV, together with the on-the-fly *ab initio* implementation described in Section VII.

A. Absorption and photoelectron spectra of ammonia

Due to its floppy nature, ammonia provides a challenging test of approximations. Absorption and photoelectron spectra of ammonia have, therefore, been used to validate new methods, such as the use of curvilinear internal coordinates (Capobianco et al., 2012) or the combination of the discrete variable representation for the large-amplitude motion and the global harmonic model for the modes orthogonal to it (Baiardi et al., 2017). The experimental $\tilde{A}^1A_2'' \leftarrow \tilde{X}^1A_1'$ ($S_1 \leftarrow S_0$) absorption spectrum of ammonia contains a single long progression due to the highly displaced umbrella mode. The nuclear configuration changes from non-planar (pyramidal) in the $\tilde{X}^1A_1'$ state to planar in the $\tilde{A}^1A_2''$ state, thus inducing a large-amplitude motion on the excited-state potential energy surface. Interestingly, the excitation of the totally symmetric N–H stretch mode, which also accompanies this electronic transition, is not observed as a separate progression (Tang et al., 1990)—this is an example of the missing-mode effect (Tutt et al., 1987).

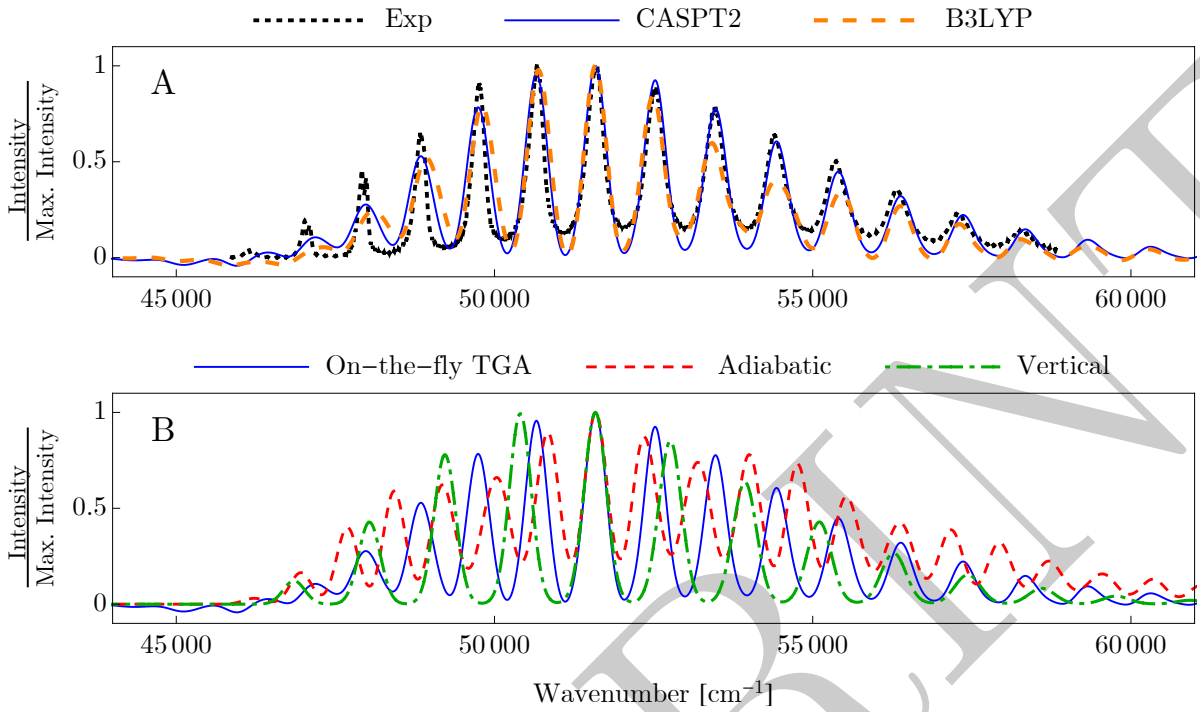

FIG. 5. Absorption spectrum of NH_3. A: Comparison of the experimental spectrum recorded at the temperature of 175 K (Chen et al., 1999) with the spectra computed with the on-the-fly *ab initio* TGA using CASPT2 and B3LYP electronic structure methods. B: Spectra evaluated using the on-the-fly, vertical harmonic, and adiabatic harmonic models (all using CASPT2). All spectra are rescaled and shifted so that the highest spectral peak in each spectrum is of unit intensity and positioned at the same wavenumber. Adapted with permission from J. Phys. Chem. A **119**, 5685 (2015). Copyright 2015 American Chemical Society.

The computation of the absorption spectrum

$$\sigma_{\rm abs}(\omega) = \frac{\omega}{3\hbar c\varepsilon_0}|\vec{\mu}_{21}|^2 {\rm Re}\int_0^\infty \langle\psi(0)|\psi(t)\rangle e^{{\rm i}(E_{1,g}/\hbar+\omega)t}{\rm d}t \tag{95}$$

involves the propagation of the initial vibrational wavepacket $|\psi(0)\rangle = |1,g\rangle$ on the excited-state potential energy surface $V_2(q)$. Equation (95) assumes the Condon approximation and accounts for the orientational averaging of the spectrum, hence the factor of three in the denominator.

Figure 5A compares the experimental spectrum with spectra calculated (Wehrle et al., 2015) with the on-the-fly *ab initio* TGA at two different levels of electronic structure theory: time-dependent density functional theory, with the B3LYP functional, and the CASPT2 method. Interestingly, the peak spacings, which are well described by the on-the-fly TGA, are not affected by the level of theory employed for the electronic structure. Unlike the on-the-fly approach, which partially includes the anharmonicity of the excited-state surface, the

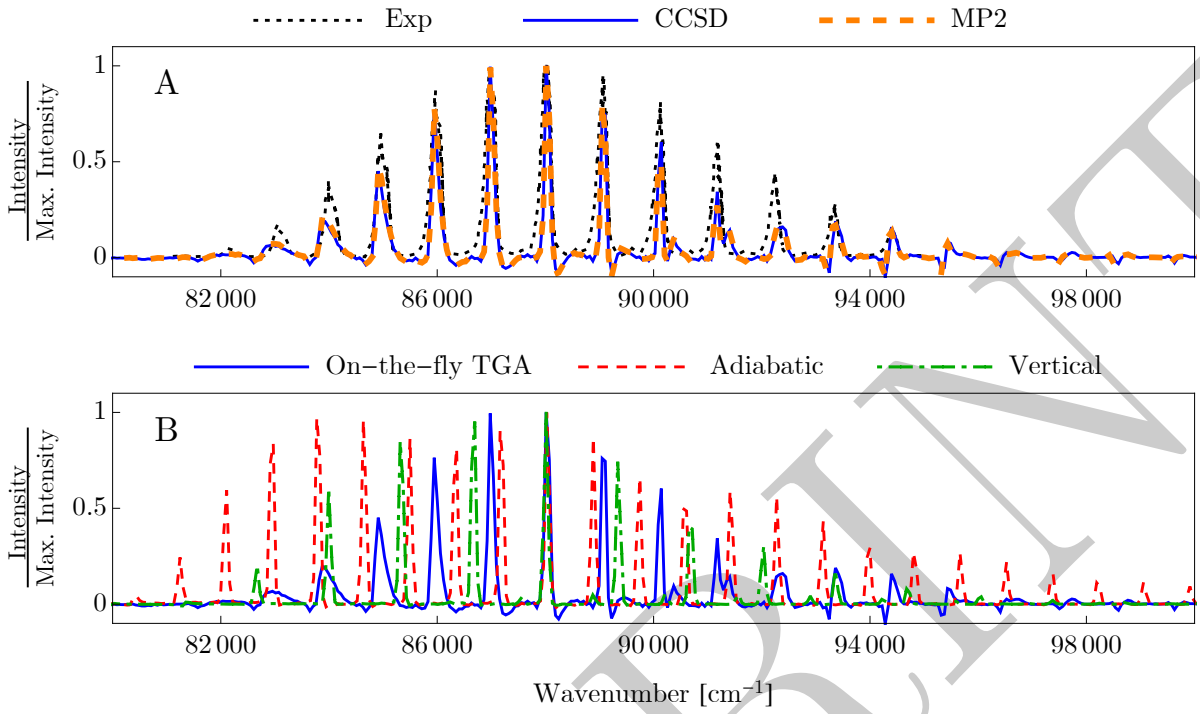

FIG. 6. Photoelectron spectrum of NH_3. A: Comparison of the experimental spectrum recorded at the temperature of 77 K (Edvardsson et al., 1999) with the spectra computed with the on-the-fly *ab initio* thawed Gaussian approximation using either the CCSD or MP2 electronic structure method. B: Comparison of the spectra evaluated with the on-the-fly, adiabatic harmonic, and vertical harmonic models (all using CCSD). All spectra are rescaled and shifted so that the highest spectral peak in each spectrum is of unit intensity and positioned at the same wavenumber. Adapted with permission from J. Phys. Chem. A **119**, 5685 (2015). Copyright 2015 American Chemical Society.

global harmonic methods fail to recover the correct shape of the spectrum (see Fig. 5B). The adiabatic harmonic model gives an inaccurate approximation of the excited-state surface, resulting in a double progression which is otherwise hidden in the experiment through the missing-mode effect. The vertical harmonic model captures at least the overall envelope of the spectrum but overestimates the frequency of the umbrella mode and, consequently, the spacings between the peaks.

Within the Condon approximation, a rotationally averaged photoelectron spectrum can be computed also with Eq. (95), but now the state 2 is a cationic state instead of an excited state of the neutral molecule (see, e.g., Lami et al. (2004)). The photoelectron spectrum of ammonia (Fig. 6) is better resolved than the absorption spectrum and, therefore, provides a more stringent test of the on-the-fly *ab initio* TGA (Wehrle et al., 2015). Yet, the TGA performs rather well. As in the absorption spectrum, the choice of the electronic structure method (Fig. 6A) affects only slightly the on-the-fly result, whereas the adiabatic harmonic

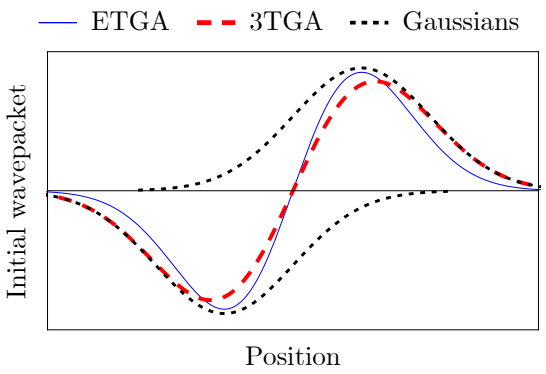

FIG. 7. Herzberg–Teller part of the wavepacket propagated with the ETGA is a Gaussian multiplied by a linear polynomial in nuclear coordinates. The 3TGA approximates the Herzberg-Teller part with two displaced Gaussians (black dotted lines). Reprinted from Chem. Phys. **515**, 152 (2018).

.

model contains spurious progressions and the vertical harmonic model completely misses the positions of the peaks (Fig. 6B).

B. Absorption spectra beyond Condon approximation

In general, the transition dipole moment is a function of nuclear coordinates, and the absorption spectrum is calculated by propagating the modified initial wavepacket $|\phi(0)\rangle = \hat{\mu}_{21}|1,g\rangle$, which includes the transition dipole moment as a factor:

$$\sigma_{\text{abs}}(\vec{\epsilon},\omega) = \frac{\omega}{\hbar c \varepsilon_0}\text{Re}\int_0^\infty \langle\phi(0)|\phi(t)\rangle e^{\text{i}(E_{1,g}/\hbar+\omega)t}\text{d}t. \tag{96}$$

As discussed in Section V D, within the Herzberg–Teller approximation, the transition dipole moment is a linear function (66) of nuclear coordinates; as a result, the initial nuclear wavefunction takes the form

$$\phi(q,0) = \left[\mu_{21}(q_0) + \partial_q\mu_{21}|_{q_0}^T \cdot (q-q_0)\right]\ \psi(q,0), \tag{97}$$

where $\psi(q,0)$ is the wavefunction (15) of the initial Gaussian state $|\psi(0)\rangle = |1,g\rangle$. Because the projection of the transition dipole moment $\mu_{21}(q) = \vec{\mu}_{21}(q)\cdot\vec{\epsilon}$ changes depending on the orientation of the molecule with respect to the polarization $\vec{\epsilon}$ of the electric field, one has to carefully average the spectrum over all orientations, as discussed in Section V E.

Wavepacket $|\phi\rangle$ can be evolved with the extended thawed Gaussian approximation, described in Section IV C (Patoz et al., 2018). The ETGA wavepacket (97) conserves its form and the corresponding parameters are propagated according to Eqs. (35) and (36). In contrast to the original TGA, the probability density at the center of the ETGA wavepacket is

not maximum, but actually vanishes. Therefore, the local harmonic approximation about the wavepacket's center becomes questionable.

To address this issue, one can use another generalization of the TGA suitable for evaluating the Herzberg–Teller spectra, but which also accounts for the wavepacket splitting. Recall that in Section IV D, we mentioned the possibility of using multiple thawed Gaussians to represent the initial wavepacket. Indeed, the Herzberg–Teller part of the initial wavepacket is well described by two displaced Gaussians of opposite sign (see Fig. 7) (Begušić et al., 2018a); the total initial wavepacket in the *three thawed Gaussians approximation* (3TGA), which also contains a Condon term, is

$$\phi^{\mathrm{3TGA}}(q,0) = \mu_{21}\, g_{q_0}(q) + f_d\, [g_{q_0+\Delta_d}(q) - g_{q_0-\Delta_d}(q)]\ . \tag{98}$$

In Eq. (98), $g_{q_c}(q)$ is a normalized Gaussian centered at q_c, with zero initial momentum and phase ($p_0 = \gamma_0 = 0$):

$$g_{q_c}(q) := N_0\ e^{\frac{i}{2\hbar}(q-q_c)^T \cdot A_0 \cdot (q-q_c)}\,, \tag{99}$$

Δ_d is a displacement vector and f_d a scaling factor ensuring normalization. The two displaced Gaussians are centered at the extrema of the Herzberg–Teller part of the initial wavepacket; note that there are always exactly two local extrema, regardless of the number D of vibrational degrees of freedom (for a proof, see Appendix E of Begušić et al. (2018a)).

An extreme case of Herzberg-Teller spectra occurs in molecules, in which the electronic transition is symmetry-forbidden, but vibronically allowed due to the nonzero elements of the gradient of the transition dipole moment (Herzberg, 1966). A prototypical example is the absorption spectrum of benzene $\tilde{\mathrm{A}}\,^1\mathrm{B}_{2\mathrm{u}} \leftarrow \tilde{\mathrm{X}}\,^1\mathrm{A}_{1\mathrm{g}}$ (Herzberg, 1966; Li et al., 2010), in which the nonzero elements, corresponding to the doubly degenerate e_{2g} vibrational modes, arise due to the nonadiabatic coupling between the first and higher excited electronic states (as discussed in Section V D and in Begušić et al. (2018a); Li et al. (2010); Quack and Merkt (2011)). The absorption spectrum contains a single progression, attributed to the totally symmetric ring-breathing mode, and a number of weak hot bands. Because the ETGA and 3TGA, as described above, do not treat finite-temperature effects, we will only discuss the peaks of the main progression.

The spectra shown in Fig. 8A imply that in benzene the local harmonic approximation holds even for the Herzberg–Teller wavepacket because the 3TGA spectrum is only slightly red-shifted (≈ 10 cm^{-1}) with respect to the ETGA spectrum (Begušić et al., 2018a). The global harmonic models (Fig. 8B) are not as accurate as the on-the-fly approach (Begušić et al., 2018a; Patoz et al., 2018). Whereas the relative intensities of adiabatic harmonic peaks have errors of 20 to 50% and the vertical harmonic model fails completely, the relative intensities of the on-the-fly peaks lie within 5% of the experimental values. Finally, Fig. 8C confirms that including the Herzberg–Teller contribution in this system is absolutely essential because the purely electronic Condon spectrum is zero.

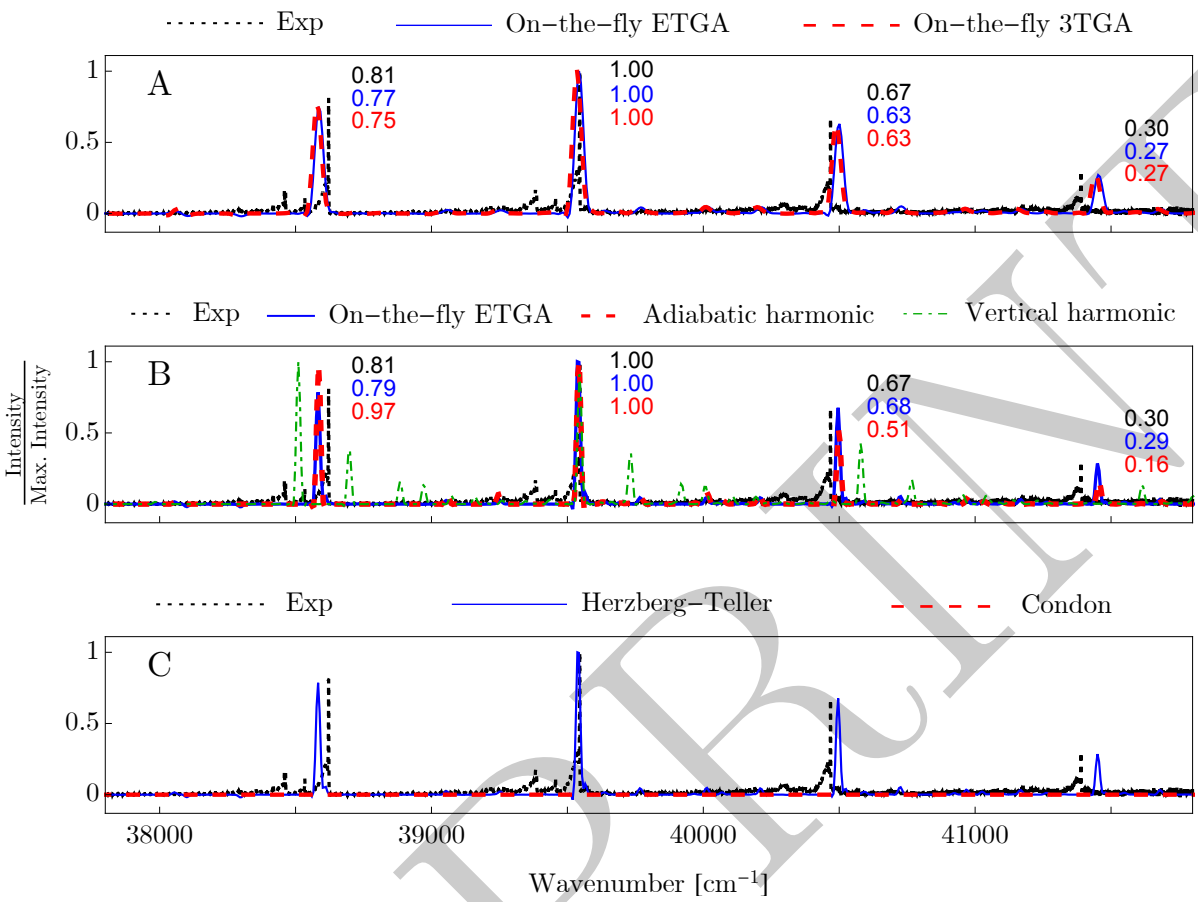

FIG. 8. Calculated absorption spectra of benzene $\tilde{A}^1B_{2u} \leftarrow \tilde{X}^1A_{1g}$ electronic transition compared to the experimental (Fally et al., 2009; Keller-Rudek et al., 2013) spectrum measured at 293 K. A: Comparison of the on-the-fly *ab initio* ETGA and 3TGA spectra. B: Comparison of the on-the-fly, adiabatic harmonic, and vertical harmonic spectra evaluated with ETGA, i.e., within the Herzberg–Teller approximation. C: Comparison of the Condon and Herzberg–Teller approximations (both evaluated using the on-the-fly approach). All spectra are horizontally shifted and rescaled according to the highest peak. To clarify the difference between the adiabatic harmonic and on-the-fly spectra, we show the scaled intensities of the experimental, adiabatic harmonic, and on-the-fly peaks. The *ab initio* calculations are based on the B3LYP/6-31+G(d,p) electronic structure method. The ETGA requires only a single trajectory, which was propagated for longer times than the trajectories used in the 3TGA. Therefore, in A, the broadening is determined by the length of the shorter 3TGA simulation, while in B and C, where only the ETGA is considered, the spectra are broadened less. A: Adapted from Chem. Phys. **515**, 152 (2018). B and C: Adapted with permission from J. Phys. Chem. Lett. **9**, 2367 (2018). Copyright 2018 American Chemical Society.

C. Emission spectra of large systems: Quinquethiophene

Computational efficiency is, of course, one of the advantages of a single- or few-trajectory methods, permitting the treatment of larger systems, which are inaccessible to multi-trajectory semiclassical methods. Wehrle et al. (2014) applied the on-the-fly *ab initio* TGA to compute the emission spectra of oligothiophenes with up to five thiophene units, i.e., up to quinquethiophene, which, due to its size (105 vibrational degrees of freedom), poses a formidable challenge to both quantum dynamical and electronic structure methods.

An emission spectrum is obtained by taking the vibrational ground state, $|2, g\rangle$, of the excited-state surface as the initial wavepacket $|\psi(0)\rangle$ and by evolving $|\phi(t)\rangle$ on the ground-state surface. Within the Condon approximation and zero-temperature limit, the *spontaneous emission* (or *fluorescence*) spectrum, measured as the rate of emission per unit frequency between ω and $\omega + \mathrm{d}\omega$, is a dimensionless quantity that can be computed as (see, e.g., Lami et al. (2004); Niu et al. (2010))

$$\sigma_{\mathrm{em}}(\omega) = \frac{\omega^3}{3\pi^2\hbar c^3 \varepsilon_0} |\vec{\mu}_{21}|^2 \,\mathrm{Re} \int_0^\infty \langle \psi(t) | \psi(0) \rangle e^{\mathrm{i}(\omega - E_{2,g}/\hbar)t} \mathrm{d}t, \tag{100}$$

where $E_{2,g}$ denotes the eigenenergy of the state $|2, g\rangle$ and $|\psi(t)\rangle = \exp(-\mathrm{i}\hat{H}_1 t/\hbar)|\psi(0)\rangle$.

Oligothiophenes, including quinquethiophene, undergo a change in symmetry upon the transition from the first excited to the ground electronic state: whereas the excited-state geometry is planar, the ground-state minimum is twisted along the inter-ring torsional degrees of freedom (see Fig. 9A). Therefore, the initial wavepacket, constructed at the minimum of the excited-state surface, starts its evolution at the top of a potential barrier of the ground-state surface. In this scenario, one could expect the exact wavepacket to split, and therefore the TGA to fail. However, due to the rather low magnitudes of the imaginary frequencies corresponding to the torsional modes, the simple spreading of the thawed Gaussian wavepacket (Fig. 9B) provides an adequate description of the dynamics along these modes, at least during the short time required for simulating the low-resolution emission spectrum (Wehrle et al., 2014). This picture is confirmed in Fig. 10A, in which the experimental and calculated spectra are shown to agree both in the positions and intensities of the peaks. (Note that, in contrast to previous examples, here the computed spectra were not shifted; a small shift between the experimental and computed peaks is most likely due to the error of electronic structure method.)

The single TGA trajectory can be used not only to evaluate the spectrum, but also to understand the spectral features and to generate partially uncoupled models (Wehrle et al., 2014) that are accessible to more rigorous quantum approaches, such as the multi-layer multi-configurational time-dependent Hartree (ML-MCTDH) method (Wang and Thoss, 2003). The reason is that the stability matrix M_t, needed in TGA, provides information about the dynamical coupling within each pair of modes. The simplified system is obtained

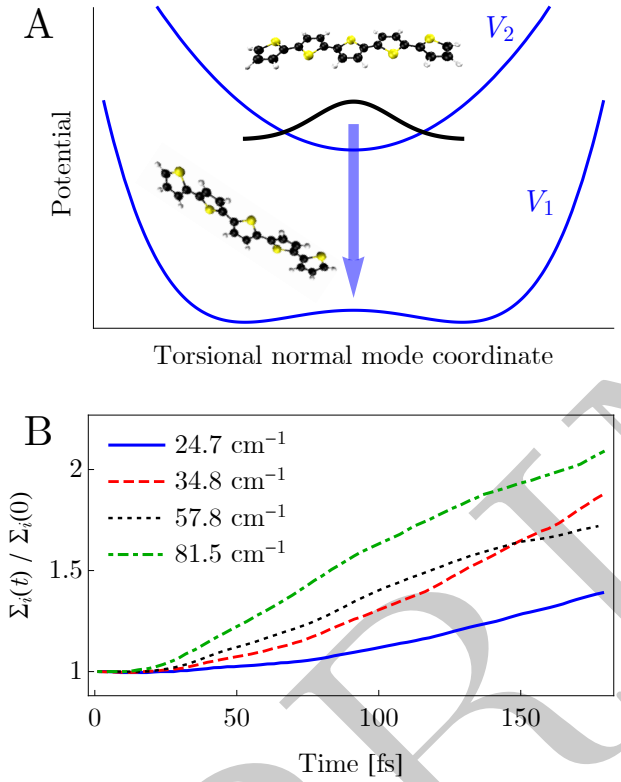

FIG. 9. Inter-ring torsional modes of quinquethiophene and the spreading of the wavepacket. A: Schematic representation of a section of the potential energy surface along one of the four torsional normal mode coordinates; the excited-state minimum has a planar configuration, whereas the ground-state minimum is twisted. B: Spreading of the wavepacket along the four inter-ring torsional degrees of freedom induced by the inverted potential. To distinguish the four modes, their excited-state wavenumbers are shown in the legend. The width of the wavepacket along the mode i is measured by the standard deviation of the probability density, $\Sigma_i(t) = (2\mathrm{Im}A_{ii,t}/\hbar)^{-1/2}$; the figure shows relative values with respect to the initial widths. B: Adapted from J. Chem. Phys. **140**, 244114 (2014), with the permission of AIP Publishing.

by neglecting the couplings below a chosen threshold (Wehrle et al., 2014); after the decoupling, the independent subsystems that contain no significantly excited modes are dropped from the analysis (Wehrle et al., 2014). Remarkably, the whole process of generating the partially uncoupled fewer-dimensional models is fully automated and thus completely avoids "chemical intuition." Comparison of the full- and reduced-dimensionality TGA calculations of quinquethiophene spectra in Fig. 10B proves that the main progression of the spectrum is generated by *only* four inter-ring-stretch and ring-squeeze modes. To account for the broadening of the peaks, it is necessary to include in the model only four additional vibrational modes, corresponding to the chain and C-H bond deformations. Overall, by including as few as eight vibrational modes, the computed spectrum reproduces very well the full 105-

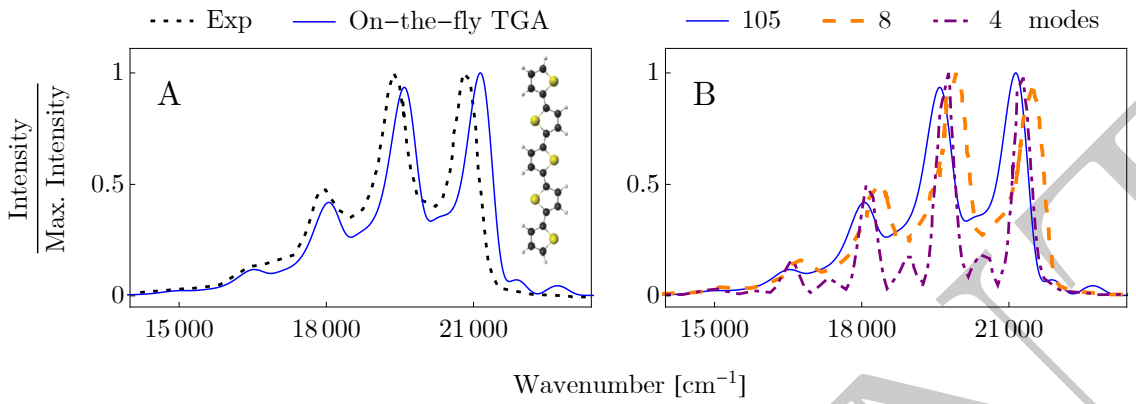

FIG. 10. Emission spectrum of quinquethiophene. A: Comparison of the experimental spectrum and the spectrum computed with the full-dimensional on-the-fly *ab initio* TGA using all 105 normal modes. B: Comparison of the spectra computed either with the full-dimensional on-the-fly *ab initio* TGA or with the TGA applied to the automatically generated reduced-dimensionality models. The spectra are labeled by the the number of normal modes treated. Adapted from J. Chem. Phys. **140**, 244114 (2014), with the permission of AIP Publishing.

dimensional result. A related "divide-and-conquer" semiclassical approach, in which the decoupling is done differently, has been used by Ceotto and coworkers to evaluate vibrational spectra of fullerene and other large systems that would be otherwise inaccessible to semiclassical initial value representation (Ceotto et al., 2017).

D. Vibrationally resolved pump-probe spectra

In a pump-probe experiment, the difference between the pump-on and pump-off spectra is measured. Within the approximations made in Section V F, the differential absorption cross-section at a probe delay time τ (often simply called the "pump-probe spectrum") is evaluated as the half-Fourier transform (Domcke and Stock, 1997; Mukamel, 1999; Pollard et al., 1990b)

$$\sigma_{\mathrm{PP}}(\vec{\epsilon}^{\,\mathrm{pu}},\vec{\epsilon}^{\,\mathrm{pr}},\omega,\tau) = \frac{4\pi^2\omega|\tilde{E}^{\mathrm{pu}}(\omega_{21})|^2}{\hbar^3 c\varepsilon_0}\,|\mu_{21}^{\mathrm{pu}}|^2 \times \mathrm{Re}\int_0^\infty \left[|\mu_{n2}^{\mathrm{pr}}|^2\,C_{\mathrm{ESA}}^*(t,\tau) - |\mu_{21}^{\mathrm{pr}}|^2\,C_{\mathrm{TRSE}}(t,\tau) - |\mu_{21}^{\mathrm{pr}}|^2\,C_{\mathrm{GSB}}(t,\tau)\right] e^{\mathrm{i}\omega t}\mathrm{d}t, \tag{101}$$

where $\mu_{\alpha\beta}^{\mathrm{pu}}$ and $\mu_{\alpha\beta}^{\mathrm{pr}}$ are the transition dipole moments $\vec{\mu}_{\alpha\beta}$ [Eq. (68)] projected onto the polarization vectors $\vec{\epsilon}^{\,\mathrm{pu}}$ and $\vec{\epsilon}^{\,\mathrm{pr}}$ of the pump and probe electric fields, and $\tilde{E}^{\mathrm{pu}}(\omega_{21})$ is the Fourier transform of the pump electric field amplitude evaluated at the transition frequency ω_{21} between the ground and excited electronic states (Begušić et al., 2018b). The three terms

in the integrand arise from three different physical processes: absorption to a higher-excited electronic state n ("excited-state absorption"),

$$C_{\mathrm{ESA}}(t,\tau) = \left\langle 1, g \left| e^{\mathrm{i}\hat{H}_2\tau/\hbar} e^{\mathrm{i}\hat{H}_n t/\hbar} e^{-\mathrm{i}\hat{H}_2(t+\tau)/\hbar} \right| 1, g \right\rangle, \tag{102}$$

time-resolved stimulated emission,

$$C_{\mathrm{TRSE}}(t,\tau) = \left\langle 1, g \left| e^{\mathrm{i}\hat{H}_2\tau/\hbar} e^{\mathrm{i}\hat{H}_1 t/\hbar} e^{-\mathrm{i}\hat{H}_2(t+\tau)/\hbar} \right| 1, g \right\rangle, \tag{103}$$

and ground-state bleach,

$$C_{\mathrm{GSB}}(t,\tau) = \left\langle 1, g \left| e^{\mathrm{i}\hat{H}_1 t/\hbar} e^{-\mathrm{i}\hat{H}_2 t/\hbar} \right| 1, g \right\rangle. \tag{104}$$

In the following discussion, we concentrate on the time-resolved stimulated emission spectrum and only in the final result we add the ground-state bleach; the excited-state absorption signal can be computed in a similar way. Although the excited-state absorption is not negligible, it is commonly found at a different frequency than the other two contributions. Therefore, the excited state absorption can be analyzed separately, unlike the ground-state bleach and stimulated emission, which often overlap (Berera et al., 2009).

As shown in Section V F, to evaluate the time-resolved stimulated emission spectrum, one must first propagate the nuclear wavepacket for time τ in the excited state, and then propagate it for time t simultaneously in both the ground and excited states [Eqs. (75) and (76)]. Within the Condon and ultrashort pulse approximations, the ground-state bleach contribution to the spectrum is much simpler to evaluate because it is equal to a scaled linear absorption spectrum discussed in Section V A.

Figure 11 shows the time-resolved stimulated emission spectrum of phenyl radical, computed with the on-the-fly *ab initio* TGA in Begušić et al. (2018b). Because the Herzberg–Teller contribution to the absorption spectrum of phenyl radical is negligible (Begušić et al., 2018a; Patoz et al., 2018), the Condon approximation was used for the time-resolved spectrum.

The spectrum exhibits oscillations over a broad range of wavenumbers, reflecting the dynamics of the wavepacket in the excited state: As the wavepacket leaves the Franck–Condon region, the energy gap decreases, shifting the spectrum towards lower wavenumbers [Eq. (113)]. Along with the changes in the position of the spectrum, the vibrational resolution also changes periodically as a function of the delay time (see Fig. 12). As the wavepacket moves away from the initial position, the spectra become broader and less resolved; the resolution of the spectrum is recovered when the wavepacket returns to the Franck–Condon region. The period of ≈ 36 fs observed in the time-resolved stimulated emission spectrum corresponds to the wavenumber of the most-displaced mode in the excited electronic state ($924\ \mathrm{cm}^{-1}$). The time-resolved stimulated emission component of the pump-probe spectrum in Fig. 11B changes significantly with the delay time τ, whereas the ground-state bleach

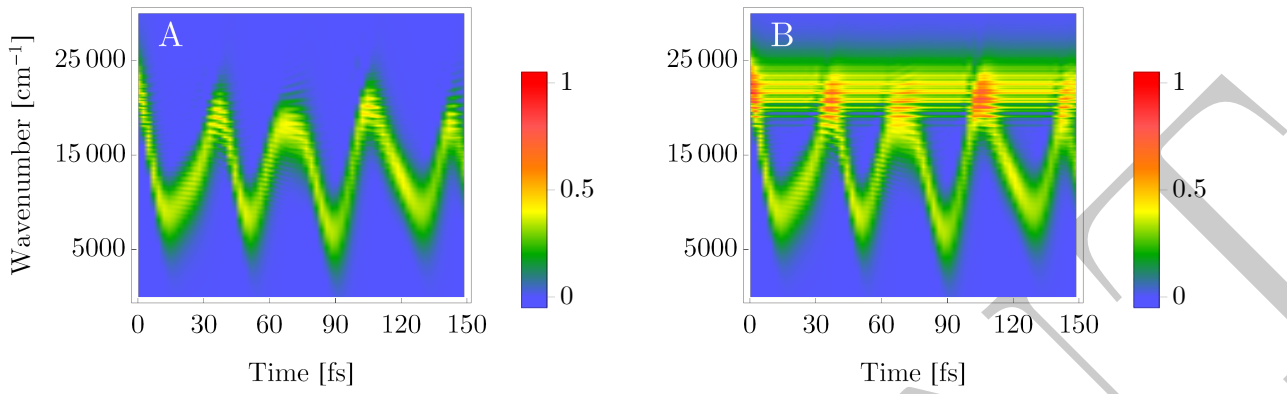

FIG. 11. Time-resolved stimulated emission spectrum (A) and the pump-probe spectrum (B) including both the stimulated emission and ground-state bleach of phenyl radical evaluated with the on-the-fly *ab initio* TGA. Both spectra were rescaled according to the maximum of the pump-probe spectrum in the right panel. *Ab initio* calculations are based on the B3LYP/SNSD (Baiardi et al., 2013) electronic structure method. Reprinted from J. Chem. Phys. **149**, 244115 (2018).

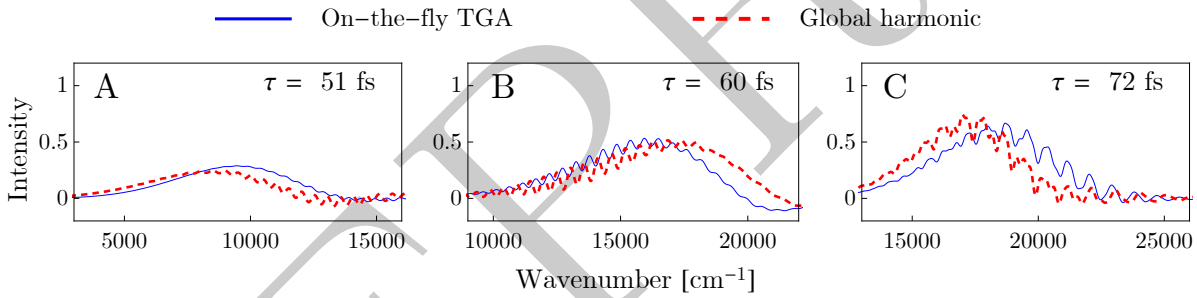

FIG. 12. Computed time-resolved stimulated emission spectra of the phenyl radical at several probe delay times τ. All spectra are scaled by the maximum of the on-the-fly spectrum at zero delay time. Adapted from J. Chem. Phys. **149**, 244115 (2018).

is constant; a similar pattern has been observed in other systems, both experimentally (Fragnito et al., 1989; van der Veen et al., 2011) and in calculations based on harmonic models (Pollard and Mathies, 1992; Pollard et al., 1990a,b).

Useful measures for analyzing the pump-probe spectra as a function of the delay time τ are the mean $\langle\omega\rangle_\tau := \int \omega\sigma_0(\omega,\tau)\mathrm{d}\omega$ and width (more precisely, standard deviation) $\Delta\omega_\tau := \sqrt{\langle\omega^2\rangle_\tau - \langle\omega\rangle_\tau^2}$ of the normalized spectral lineshapes (Ferrer et al., 2013; Pollard et al., 1990b)

$$\sigma_0(\omega,\tau) = \frac{\sigma_{\mathrm{PP}}(\omega,\tau)/\omega}{\int(\sigma_{\mathrm{PP}}(\omega,\tau)/\omega)\mathrm{d}\omega}. \tag{105}$$

Both quantities can be expressed in terms of the energy gap operator $\Delta\hat{V} = \hat{V}_2 - \hat{V}_1$ and the excited-state wavepacket $|\psi(\tau)\rangle = |\psi_\alpha(0,\tau)\rangle$ [Eq. 76] at time τ. The mean of the spectrum

is determined by the expectation value of the energy gap (Pollard et al., 1990b),

$$\langle\omega\rangle_\tau = \frac{1}{\hbar}\langle\psi(\tau)|\Delta\hat{V}|\psi(\tau)\rangle, \tag{106}$$

while the width is given by the standard deviation of the energy gap (Pollard et al., 1990b):

$$\Delta\omega_\tau = \frac{1}{\hbar}\sqrt{\langle\psi(\tau)|\Delta\hat{V}^2|\psi(\tau)\rangle - \langle\psi(\tau)|\Delta\hat{V}|\psi(\tau)\rangle^2}. \tag{107}$$

For a thawed Gaussian wavepacket $\psi(\tau)$ and within the local harmonic approximation, the mean and width of the spectra can be evaluated analytically (Begušić et al., 2018b) as

$$\langle\omega\rangle_\tau^{\mathrm{LHA}} = \frac{1}{\hbar}[\Delta V_\tau + \frac{1}{2}\,\mathrm{Tr}(\Delta V_\tau'' \cdot \Sigma_\tau^2)], \tag{108}$$

$$\Delta\omega_\tau^{\mathrm{LHA}} = \frac{1}{\hbar}\sqrt{(\Delta V_\tau')^T \cdot \Sigma_\tau^2 \cdot \Delta V_\tau' + \frac{1}{2}\,\mathrm{Tr}(\Delta V_\tau'' \cdot \Sigma_\tau^2 \cdot \Delta V_\tau'' \cdot \Sigma_\tau^2)}, \tag{109}$$

where ΔV_τ, $\Delta V_\tau'$, $\Delta V_\tau''$ are, respectively, the energy gap, its gradient, and Hessian evaluated at the center q_τ of the wavepacket at time τ:

$$\Delta V_\tau = V_2|_{q_\tau} - V_1|_{q_\tau}, \tag{110}$$

$$\Delta V_\tau' = \mathrm{grad}_q\, V_2|_{q_\tau} - \mathrm{grad}_q\, V_1|_{q_\tau}, \tag{111}$$

$$\Delta V_\tau'' = \mathrm{Hess}_q V_2|_{q_\tau} - \mathrm{Hess}_q V_1|_{q_\tau}. \tag{112}$$

Remarkably, evaluating the mean and width of the pump-probe spectrum from expressions (106)–(107) does not require running trajectories on the ground surface; this is only necessary if the full, frequency-resolved spectrum is wanted.

If the two potential surfaces have similar curvatures ($\Delta V_\tau'' \approx 0$), then Eqs. (108) and (109) simplify further to:

$$\langle\omega\rangle_\tau^{\mathrm{appr}} = \Delta V_\tau/\hbar \tag{113}$$

$$\Delta\omega_\tau^{\mathrm{appr}} = \frac{1}{\hbar}\sqrt{(\Delta V_\tau')^T \cdot \Sigma_\tau^2 \cdot \Delta V_\tau'}. \tag{114}$$

According to Eq. (113), the mean of the spectrum can be computed by evaluating the energy gap along a single excited-state classical trajectory. The widths of the spectra, however, require the full TGA propagation on the excited-state surface as well as the ground-state gradients along the excited-state trajectory.

Comparison between the global harmonic and the more accurate on-the-fly results (see Fig. 12) indicates the presence of anharmonicity effects. In spite of a very good description of the mean of the spectrum (see Fig. 13), the global harmonic approximation completely loses the accuracy of the frequency-resolved features. Moreover, the success of the global harmonic approximation in describing at least the mean of the spectra is due to a partial error cancellation arising from omitting anharmonicity in both potential energy surfaces.

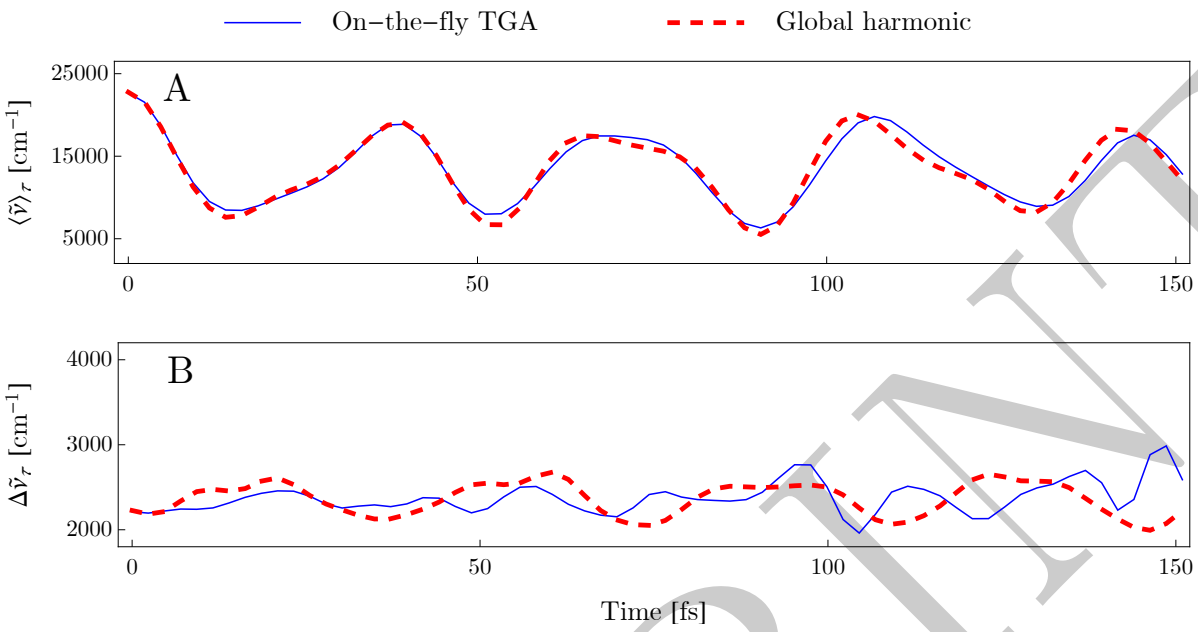

FIG. 13. Means (A) and widths (B) of the computed time-resolved stimulated emission spectra of the phenyl radical. Adapted from J. Chem. Phys. **149**, 244115 (2018).

IX. CONCLUSION AND OUTLOOK

In this chapter, we have discussed one of many possible approaches to the calculation of vibrationally resolved electronic spectra of molecules: The on-the-fly *ab initio* semiclassical thawed Gaussian approximation avoids constructing a global potential energy surface by evaluating the potential energy, its gradient, and Hessian only where needed along a classical trajectory and, moreover, takes into account all degrees of freedom. At the other extreme are approaches using exact quantum propagation on reduced-dimensionality surfaces, globally harmonic surfaces, or other approximate surfaces such as those with the potential energy function expressed in the "sum-of-products" form.

The very simple TGA cannot compete with the accuracy of exact quantum methods if those are feasible in a given system. Yet, the TGA has two properties of central importance for molecular quantum dynamics and, in particular, for evaluating vibrationally resolved electronic spectra: First, the TGA is exact in a globally harmonic potential, which is often a decent starting point for approximating the exact potential energy surface of a rigid molecule. Moreover, the TGA performs well in nearly-harmonic potentials, outperforming the global harmonic approaches by including anharmonicity at least partially. Second, the TGA is exact in the short-time limit and, in practice, accurate at times before the wavepacket splitting takes place; this is often sufficient for describing low-resolution vibronic and ultrafast time-resolved spectra.

In Section VIII, we have shown several examples of on-the-fly *ab initio* calculations of both steady-state and time-resolved molecular electronic spectra. Surprisingly, the Condon absorption and photoelectron spectra computed with the TGA are accurate even in the rather floppy molecule of ammonia. We have mentioned two extensions of the TGA for evaluating spectra beyond the Condon approximation. Both the extended TGA and the 3TGA allow the treatment of Herzberg-Teller spectra of fairly large molecules. In benzene and other molecules in which wavepacket splitting is negligible, the spectra are well described with the simpler, one-trajectory ETGA, at a cost of the original TGA. As shown on the emission spectrum of quinquethiophene, the on-the-fly *ab initio* TGA is feasible in rather large molecules. In this particular system, the accuracy of the spectrum is not corrupted by the double-well nature of the potential energy surface, which justifies using the Gaussian wavepacket ansatz in the simulation of low-resolution electronic spectra. On the quinquethiophene example, we have also shown that the single-trajectory TGA would be useful even if its accuracy were unsatisfactory; when this happens, the reduced-dimensionality models generated through the automatic decoupling procedure can be subsequently treated with more accurate semiclassical or exact quantum dynamical methods. A similar automated "divide and conquer" approach, based on somewhat different criteria for the decoupling, was used successfully by Ceotto and coworkers for computing vibrational spectra (Ceotto et al., 2017). The last of the examples, namely the pump-probe spectrum of the phenyl radical, proves that the on-the-fly *ab initio* calculations are feasible even when more trajectories are required and that the blind application of global harmonic models is dangerous: Due to cancellation of errors between the ground and excited states, the global harmonic models can yield accurate observables, such as means of spectra, even in anharmonic systems whose vibrationally resolved spectra are strongly affected by the anharmonicity.

Because the TGA and its extensions mentioned in this chapter require only a single or few classical trajectories, along with the corresponding Hessians, such methods allow an on-the-fly implementation in conjunction with rather high-level *ab initio* electronic structure calculations. In contrast, many-trajectory approaches such as the variants of the Herman-Kluk initial value representation, on one hand result in more accurate nuclear dynamics, but, on the other hand, require many trajectories for convergence, which makes them practical only with less accurate electronic structure methods. Overall, it seems that until on-the-fly *ab initio* many-trajectory approaches become more efficient, the TGA will remain an interesting option for evaluating spectra of slightly anharmonic molecules. Therefore, it is also worthwhile to explore ways to eliminate the shortcomings of the TGA without increasing too much the computational cost.

The local harmonic approximation, employed in the TGA, holds as long as the wavepacket is compact because wavepacket spreading leads to incorrect description of the potential at its tails. Consequently, the single Gaussian wavepacket ansatz cannot describe wavepacket

splitting or tunneling through barriers. Yet, when the initial wavepacket happens to land on the top of a potential barrier, which happens in many molecules, the splitting is inevitable. Typical examples are provided by the absorption spectrum of formaldehyde (Bonfanti et al., 2018; Tatchen and Pollak, 2009) and emission spectrum of ammonia (Tang et al., 1991). In ammonia, wavepacket splitting is captured at least qualitatively by representing the initial wavepacket as a sum of two Gaussians slightly displaced along the floppy mode. The resulting emission spectrum includes also the progression assigned to the low-frequency umbrella mode, whereas the single-trajectory TGA reproduces only the N-H stretch progression (Begušić et al.).

Another possible target for improvement is a further reduction of the computational cost by exploring different approximations to the Hessians needed in the thawed Gaussian propagation, such as Hessian updating (Ceotto et al., 2013; Zhuang et al., 2013) or interpolation schemes. An extreme possibility is using only one Hessian for the whole propagation. Note that this is different from a global harmonic approximation because the single-Hessian approximation will affect only the wavepacket width and phase, while the center of the wavepacket will follow the exact, anharmonic on-the-fly classical trajectory, as in the original TGA. Such an approximation can be useful when dealing with very large systems, where the quadratic scaling of the Hessian calculations becomes the computational bottleneck. Remarkably, using only one Hessian for the thawed Gaussian propagation decouples the classical propagation of the center of the wavepacket [Eqs. (18) and (19)] from the semiclassical part [Eqs. (20) and (21)], resulting in a higher-dimensional classical Hamiltonian structure and rigorous conservation of energy (Begušić et al., 2019), neither of which is true in the original TGA.

As for the time-resolved spectra calculations, the discussion in Sections V F and VIII D did not take into account finite pulse duration. If the pulses are much shorter than the vibrational period, this ultrashort pulse approximation is valid; however, when the time resolution is lower, the oscillations in the spectra corresponding to high-frequency vibrational modes disappear. In most experiments, the pulse duration is in the impulsive limit (i.e., satisfies the ultrashort pulse approximation) only for the low-frequency vibrational modes, while the dynamics in the faster modes is not observed. To account for pulse duration in the TGA and therefore permit a more direct comparison with experiment, all one has to do is extend the pump-probe methodology from Section VIII D by evaluating the third-order response function (Begušić and Vaníček) and then convolving it with the pulse envelopes (Pollard and Mathies, 1992).

In conclusion, we believe that, despite its age and simplicity, it is too early to discard the TGA and that, thanks to their simplicity, on-the-fly *ab initio* calculations in general, and TGA in particular, can be useful not only for the interpretation of existing experimental data, but also for the design of new experiments. Finally, we would like to acknowledge the

support from European Research Council (ERC) under the European Union's Horizon 2020 research and innovation programme (grant agreement No. 683069 – MOLEQULE).

J. P. Alborzpour, D. P. Tew, and S. Habershon. Efficient and accurate evaluation of potential energy matrix elements for quantum dynamics using Gaussian process regression. *J. Chem. Phys.*, 145(17):174112, 2016. doi:10.1063/1.4964902.

D. L. Andrews and T. Thirunamachandran. On three-dimensional rotational averages. *J. Chem. Phys.*, 67(11):5026–5033, 1977. doi:10.1063/1.434725.

S. V. Antipov, Z. Ye, and N. Ananth. Dynamically consistent method for mixed quantum-classical simulations: a semiclassical approach. *J. Chem. Phys.*, 142:184102, 2015. doi:10.1063/1.4919667. URL `http://aip.scitation.org/doi/abs/10.1063/1.4919667`.

F. J. Avila Ferrer and F. Santoro. Comparison of vertical and adiabatic harmonic approaches for the calculation of the vibrational structure of electronic spectra. *Phys. Chem. Chem. Phys.*, 14 (39):13549–13563, 2012. doi:10.1039/c2cp41169e.

M. Baer. *Beyond Born-Oppenheimer: Electronic Nonadiabatic Coupling Terms and Conical Intersections*. Wiley, 1 edition, 2006. ISBN 978-0-471-77891-2.

A. Baiardi, J. Bloino, and V. Barone. General time dependent approach to vibronic spectroscopy including Franck-Condon, Herzberg-Teller, and Duschinsky effects. *J. Chem. Theory Comput.*, 9 (9):4097–4115, 2013. doi:10.1021/ct400450k.

A. Baiardi, J. Bloino, and V. Barone. Simulation of Vibronic Spectra of Flexible Systems: Hybrid DVR-Harmonic Approaches. *J. Chem. Theory Comput.*, 13(6):2804–2822, 2017. doi: 10.1021/acs.jctc.7b00236.

T. Begušić and J. Vaníček. Unpublished.

T. Begušić, Z. T. Zhang, S. Choi, and J. Vaníček. Unpublished.

T. Begušić, A. Patoz, M. Šulc, and J. Vaníček. On-the-fly ab initio three thawed Gaussians approximation: a semiclassical approach to Herzberg-Teller spectra. *Chem. Phys.*, 515:152–163, 2018a. doi:https://doi.org/10.1016/j.chemphys.2018.08.003.

T. Begušić, J. Roulet, and J. Vaníček. On-the-fly ab initio semiclassical evaluation of time-resolved electronic spectra. *J. Chem. Phys.*, 149:244115, 2018b.

T. Begušić, M. Cordova, and J. Vaníček. Single-Hessian thawed Gaussian approximation. *J. Chem. Phys.*, 2019. doi:10.1063/1.5090122.

R. Berera, R. van Grondelle, and J. T. M. Kennis. Ultrafast transient absorption spectroscopy: principles and application to photosynthetic systems. *Photosynthesis Research*, 101 (2–3):105–118, 2009. doi:10.1007/s11120-009-9454-y. URL `http://link.springer.com/10.1007/s11120-009-9454-y`.

M. P. Bircher, E. Liberatore, N. J. Browning, S. Brickel, C. Hofmann, A. Patoz, O. T. Unke, T. Zimmermann, M. Chergui, P. Hamm, U. Keller, M. Meuwly, H. J. Woerner, J. Vaníček, and U. Rothlisberger. Nonadiabatic effects in electronic and nuclear dynamics. *Struct. Dyn.*, 4(6):

061510, 2017. ISSN 23297778. doi:10.1063/1.4996816.

M. Bonfanti, J. Petersen, P. Eisenbrandt, I. Burghardt, and E. Pollak. Computation of the S1 S0 vibronic absorption spectrum of formaldehyde by variational Gaussian wavepacket and semiclassical IVR methods. *J. Chem. Theory Comput.*, 14:5310–4323, 2018. doi:10.1021/acs.jctc.8b00355.

M. Buchholz, F. Grossmann, and M. Ceotto. Mixed semiclassical initial value representation time-averaging propagator for spectroscopic calculations. *The Journal of Chemical Physics*, 144(9): 094102, 2016. doi:10.1063/1.4942536.

A. Capobianco, R. Borrelli, C. Noce, and A. Peluso. Franck-Condon factors in curvilinear coordinates: The photoelectron spectrum of ammonia. *Theor. Chem. Acc.*, 131(3):1–10, 2012. doi: 10.1007/s00214-012-1181-3.

M. Ceotto, S. Atahan, S. Shim, G. F. Tantardini, and A. Aspuru-Guzik. First-principles semiclassical initial value representation molecular dynamics. *Phys. Chem. Chem. Phys.*, 11:3861–3867, 2009a. doi:10.1039/B820785B. URL `http://dx.doi.org/10.1039/B820785B`.

M. Ceotto, S. Atahan, G. F. Tantardini, and A. Aspuru-Guzik. Multiple coherent states for first-principles semiclassical initial value representation molecular dynamics. *J. Chem. Phys.*, 130(23): 234113, 2009b. doi:10.1063/1.3155062. URL `http://link.aip.org/link/?JCP/130/234113/1`.

M. Ceotto, G. F. Tantardini, and A. Aspuru-Guzik. Fighting the curse of dimensionality in first-principles semiclassical calculations: Non-local reference states for large number of dimensions. *J. Chem. Phys.*, 135(21):214108, 2011. doi:10.1063/1.3664731. URL `http://link.aip.org/link/?JCP/135/214108/1`.

M. Ceotto, Y. Zhuang, and W. L. Hase. Accelerated direct semiclassical molecular dynamics using a compact finite difference hessian scheme. *J. Chem. Phys.*, 138(5):054116, 2013. doi: 10.1063/1.4789759. URL `http://link.aip.org/link/?JCP/138/054116/1`.

M. Ceotto, G. Di Liberto, and R. Conte. Semiclassical "divide-and-conquer" method for spectroscopic calculations of high dimensional molecular systems. *Phys. Rev. Lett.*, 119:010401, Jul 2017.

F. Chen, D. Judge, C. Wu, and J. Caldwell. Low and room temperature photoabsorption cross sections of NH3 in the UV region. *Planet. Space Sci.*, 47(1-2):261–266, 1999. doi:10.1016/S0032-0633(98)00074-9.

M. S. Child and D. V. Shalashilin. Locally coupled coherent states and Herman-Kluk dynamics. *J. Chem. Phys.*, 118(5):2061–2071, 2003. doi:10.1063/1.1531997.

M. S. Church, S. V. Antipov, and N. Ananth. Validating and implementing modified filinov phase filtration in semiclassical dynamics. *J. Chem. Phys.*, 146:234104, 2017.

E. Condon. A theory of intensity distribution in band systems. *Phys. Rev.*, 28(6):1182–1201, 1926. doi:10.1103/PhysRev.28.1182.

E. U. Condon. Coupling of electronic and nuclear motions in diatomic molecules. *Proc. Nat. Acad. Sci. USA*, 13:462 – 466, 1927.

E. U. Condon. Nuclear motions associated with electron transitions in diatomic molecules. *Phys. Rev.*, 32:858 – 872, 1928.

E. A. Coutsias, C. Seok, and K. A. Dill. Using quaternions to calculate rmsd. *J. Comput. Chem.*, 25(15):1849–1857, 2004. doi:10.1002/jcc.20110. URL `https://onlinelibrary.wiley.com/doi/abs/10.1002/jcc.20110`.

B. F. E. Curchod and T. J. Martínez. Ab initio nonadiabatic quantum molecular dynamics. *Chem. Rev.*, 118(7):3305–3336, 2018.

W. Domcke and G. Stock. Theory of Ultrafast Nonadiabatic Excited-State Processes and their Spectroscopic Detection in Real Time. *Adv. Chem. Phys.*, 100:1–169, 1997. doi: 10.1002/9780470141595.ch1.

W. Domcke and D. R. Yarkony. Role of conical intersections in molecular spectroscopy and photoinduced chemical dynamics. *Annu. Rev. Phys. Chem.*, 63(1):325–352, 2012. doi: 10.1146/annurev-physchem-032210-103522. URL `http://www.annualreviews.org/doi/abs/10.1146/annurev-physchem-032210-103522`.

D. Edvardsson, P. Baltzer, L. Karlsson, B. Wannberg, D. M. P. Holland, D. A. Shaw, and E. E. Rennie. A photoabsorption, photodissociation and photoelectron spectroscopy study of NH3 and ND3. *J. Phys. B: At. Mol. Opt. Phys.*, 32(11):2583–2609, 1999. doi:10.1088/0953-4075/32/11/309.

F. Egidi, J. Bloino, C. Cappelli, and V. Barone. A robust and effective time-independent route to the calculation of resonance Raman spectra of large molecules in condensed phases with the inclusion of Duschinsky, Herzberg-Teller, anharmonic, and environmental effects. *J. Chem. Theory Comput.*, 10(1):346–363, 2014. doi:10.1021/ct400932e.

S. A. Egorov, E. Rabani, and B. J. Berne. Vibronic spectra in condensed matter: A comparison of exact quantum mechanical and various semiclassical treatments for harmonic baths. *J. Chem. Phys.*, 108(4):1407–1422, 1998. doi:10.1063/1.475512. URL `http://link.aip.org/link/?JCP/108/1407/1`.

S. A. Egorov, E. Rabani, and B. J. Berne. Nonradiative relaxation processes in condensed phases: Quantum versus classical baths. *J. Chem. Phys.*, 110(11):5238–5248, 1999. doi:10.1063/1.478420. URL `http://link.aip.org/link/?JCP/110/5238/1`.

S. Fally, M. Carleer, and A. C. Vandaele. Uv fourier transform absorption cross sections of benzene, toluene, meta-, ortho-, and para-xylene. *J. Quant. Spectrosc. Radiat. Transf.*, 110(9-10):766–782, 2009. doi:10.1016/j.jqsrt.2008.11.014.

E. Faou, V. Gradinaru, and C. Lubich. Computing semiclassical quantum dynamics with Hagedorn wavepackets. *SIAM J. Sci. Comput.*, 31(4):3027–3041, 2009.

F. J. Ferrer, J. Cerezo, E. Stendardo, R. Improta, and F. Santoro. Insights for an accurate comparison of computational data to experimental absorption and emission spectra: Beyond the vertical transition approximation. *J. Chem. Theory Comput.*, 9(4):2072–2082, 2013. doi: 10.1021/ct301107m.

M. Fortino, J. Bloino, E. Collini, L. Bolzonello, M. Trapani, F. Faglioni, and A. Pedone. On the simulation of vibrationally resolved electronic spectra of medium-size molecules: the case of styryl substituted BODIPYs. *Phys. Chem. Chem. Phys.*, pages 5–15, 2019. doi:10.1039/C8CP02845A.

H. L. Fragnito, J. Y. Bigot, P. C. Becker, and C. V. Shank. Evolution of the vibronic absorption spectrum in a molecule following impulsive excitation with a 6 fs optical pulse. *Chem. Phys. Lett.*, 160(2):101–104, 1989.

J. Franck and E. G. Dymond. Elementary processes of photochemical reactions. *Trans. Faraday Soc.*, 21(February):536–542, 1926. doi:10.1039/TF9262100536. URL `http://dx.doi.org/10.1039/TF9262100536`.

F. Gabas, R. Conte, and M. Ceotto. On-the-fly ab initio semiclassical calculation of glycine vibrational spectrum. *J. Chem. Theory Comput.*, 13(6):2378, 2017. URL `http://pubs.acs.org/doi/abs/10.1021/acs.jctc.6b01018`.

M. F. Gelin, R. Borrelli, and W. Domcke. Efficient orientational averaging of nonlinear optical signals in multi-chromophore systems. *J. Chem. Phys.*, 147(4):044114, 2017.

R. J. Glauber. Theory of Optical Coherence. *Physical Review*, 130(6):2529–2539, 1963. doi:10.1103/PhysRev.130.2529.

T. Gorin, T. Prosen, T. H. Seligman, and M. Žnidarič. Dynamics of loschmidt echoes and fidelity decay. *Phys. Rep.*, 435(2-5):33–156, 2006. doi:10.1016/j.physrep.2006.09.003. URL `http://www.sciencedirect.com/science/article/pii/S0370157306003310`.

G. A. Hagedorn. Semiclassical quantum mechanics. I. The $\hbar \to 0$ limit for coherent states. *Commun. Math. Phys.*, 71(1):77–93, 1980.

E. J. Heller. Time-dependent approach to semiclassical dynamics. *J. Chem. Phys.*, 62(4):1544–1555, feb 1975. doi:10.1063/1.430620. URL `http://dx.doi.org/10.1063/1.430620`.

E. J. Heller. Classical s-matrix limit of wave packet dynamics. *J. Chem. Phys.*, 65(11):4979–4989, 1976. doi:10.1063/1.432974. URL `http://link.aip.org/link/?JCP/65/4979/1`.

E. J. Heller. Frozen gaussians: A very simple semiclassical approximation. *J. Chem. Phys.*, 75 (6):2923–2931, 1981a. doi:10.1063/1.442382. URL `http://aip.scitation.org/doi/10.1063/1.442382`.

E. J. Heller. The semiclassical way to molecular spectroscopy. *Acc. Chem. Res.*, 14(12):368–375, 1981b. doi:10.1021/ar00072a002. URL `http://pubs.acs.org/doi/abs/10.1021/ar00072a002`.

E. J. Heller. Cellular dynamics: A new semiclassical approach to time-dependent quantum mechanics. *J. Chem. Phys.*, 94(4):2723–2729, 1991. doi:10.1063/1.459848. URL `http://link.aip.org/link/?JCP/94/2723/1`.

E. J. Heller. *The semiclassical way to dynamics and spectroscopy.* Princeton University Press, Princeton, NJ, 2018.

M. F. Herman and E. Kluk. A semiclasical justification for the use of non-spreading wavepackets in dynamics calculations. *Chem. Phys.*, 91(1):27–34, 1984. ISSN 0301-0104. doi:

10.1016/0301-0104(84)80039-7. URL http://www.sciencedirect.com/science/article/pii/0301010484800397.

G. Herzberg. *Molecular Spectra and Molecular Structure: III. Electronic Spectra of Polyatomic Molecules*. D.Van Nostrand Company Inc., 1966.

G. Herzberg and E. Teller. Schwingungsstruktur der elektronenübergänge bei mehratomigen molekülen. *Z. Phys. Chem. B*, 21(5-6):410, 1933.

R. Ianconescu, J. Tatchen, and E. Pollak. On-the-fly semiclassical study of internal conversion rates of formaldehyde. *J. Chem. Phys.*, 139(15):154311, 2013. doi:http://dx.doi.org/10.1063/1.4825040. URL http://scitation.aip.org/content/aip/journal/jcp/139/15/10.1063/1.4825040.

W. Kabsch. A discussion of the solution for the best rotation to relate two sets of vectors. *Acta Cryst. A*, 34(5):827–828, 1978. doi:10.1107/S0567739478001680. URL https://doi.org/10.1107/S0567739478001680.

A. L. Kaledin and W. H. Miller. Time averaging the semiclassical initial value representation for the calculation of vibrational energy levels. *J. Chem. Phys.*, 118(16):7174–7182, 2003. doi:10.1063/1.1562158. URL http://link.aip.org/link/?JCP/118/7174/1.

K. G. Kay. Semiclassical initial value treatments of atoms and molecules. *Annu. Rev. Phys. Chem.*, 56(1):255–280, 2005. doi:10.1146/annurev.physchem.56.092503.141257. URL http://www.annualreviews.org/doi/abs/10.1146/annurev.physchem.56.092503.141257.

S. K. Kearsley. On the orthogonal transformation used for structural comparisons. *Acta Cryst. A*, 45:208–210, 1989. doi:10.1107/S0108767388010128.

H. Keller-Rudek, G. K. Moortgat, R. Sander, and R. Sörensen. The MPI-Mainz UV/VIS spectral atlas of gaseous molecules of atmospheric interest. *Earth Syst. Sci. Data*, 5(2):365–373, 2013. doi:10.5194/essd-5-365-2013. URL http://www.earth-syst-sci-data.net/5/365/2013/.

J. R. Klauder and B.-S. Skagerstam. *Coherent States*. World Scientific Publishing, Singapore, 1985. ISBN 978-9971966539. doi:10.1142/0096.

K. N. Kudin and A. Y. Dymarsky. Eckart axis conditions and the minimization of the root-mean-square deviation: Two closely related problems. *J. Chem. Phys.*, 122(22):224105, 2005. doi:10.1063/1.1929739. URL http://link.aip.org/link/?JCP/122/224105/1.

A. Lami, C. Petrongolo, and F. Santoro. Absorption, emission, and photoelectron continuous-wave spectra. In W. Domcke, D. R. Yarkony, and H. Köppel, editors, *Conical intersections: Electronic structure, dynamics and spectroscopy*, chapter 16, pages 699–738. World Scientific Publishing, Singapore, 2004. doi:10.1142/5406.

G. Laude, D. Calderini, D. P. Tew, and J. O. Richardson. Ab initio instanton rate theory made efficient using Gaussian process regression. *Faraday Discuss.*, 212:237–258, 2018. doi:10.1039/C8FD00085A.

S.-Y. Lee and E. J. Heller. Exact time-dependent wave packet propagation: Application to the photodissociation of methyl iodide. *J. Chem. Phys.*, 76(6):3035–3044, 1982. doi:10.1063/1.443342.

URL http://link.aip.org/link/?JCP/76/3035/1.

B. G. Levine and T. J. Martinez. Isomerization through conical intersections. *Annu. Rev. Phys. Chem.*, 58:613–634, 2007.

B. Li, C. Mollica, and J. Vaníček. Efficient evaluation of accuracy of molecular quantum dynamics using dephasing representation. *J. Chem. Phys.*, 131(4):041101, 2009. doi:10.1063/1.3187240. URL http://link.aip.org/link/?JCP/131/041101/1.

J. Li, C.-K. Lin, X. Y. Li, C. Y. Zhu, and S. H. Lin. Symmetry forbidden vibronic spectra and internal conversion in benzene. *Phys. Chem. Chem. Phys.*, 12(45):14967–76, 2010. doi: 10.1039/c0cp00120a. URL http://www.ncbi.nlm.nih.gov/pubmed/20949142.

Z. Li, J.-Y. Fang, and C. C. Martens. Simulation of ultrafast dynamics and pump–probe spectroscopy using classical trajectories. *J. Chem. Phys.*, 104(18):6919–6929, 1996. doi: 10.1063/1.471407. URL http://link.aip.org/link/?JCP/104/6919/1.

R. MacKenzie, M. Pineault, and L. Renaud-Desjardins. Optimizing adiabaticity in quantum mechanics. *Canad. J. Phys.*, 90(2):187, 2012. doi:10.1139/p2012-005.

N. Makri and W. H. Miller. Monte carlo path integration for the real time propagator. *J. Chem. Phys.*, 89:2170–2177, 1988.

R. Marquardt and M. Quack. Infrared-multiphoton excitation and wave packet motion of the harmonic and anharmonic oscillators: Exact solutions and quasiresonant approximation. *J. Chem. Phys.*, 90(11):6320–6327, 1989. doi:10.1063/1.456348.

W. H. Miller. Classical S matrix: Numerical application to inelastic collisions. *J. Chem. Phys.*, 53(9):3578–3587, 1970. doi:10.1063/1.1674535. URL http://scitation.aip.org/content/aip/journal/jcp/53/9/10.1063/1.1674535.

W. H. Miller. The semiclassical initial value representation: A potentially practical way for adding quantum effects to classical molecular dynamics simulations. *J. Phys. Chem. A*, 105(13):2942, 2001.

S. Mukamel. On the semiclassical calculation of molecular absorption and fluorescence spectra. *J. Chem. Phys.*, 77(1):173–181, 1982. doi:10.1063/1.443638. URL http://link.aip.org/link/?JCP/77/173/1.

S. Mukamel. *Principles of nonlinear optical spectroscopy*. Oxford University Press, New York, 1 edition, 1999. ISBN 978-0195092783.

S. Mukamel. Multidimensional femtosecond correlation spectroscopies of electronic and vibrational excitations. *Annu. Rev. Phys. Chem.*, 51:691 – 729, 2000.

H. Nakamura. *Nonadiabatic Transition: Concepts, Basic Theories and Applications*. World Scientific Publishing Company, 2 edition, 2012. ISBN 978-981-4329-77-4.

Y. Niu, Q. Peng, C. Deng, X. Gao, and Z. Shuai. Theory of excited state decays and optical spectra: Application to polyatomic molecules. *J. Phys. Chem. A*, 114(30):7817–7831, 2010. doi: 10.1021/jp101568f.

H. M. Pastawski, P. R. Levstein, G. Usaj, J. Raya, and J. Hirschinger. A nuclear magnetic resonance answer to the boltzmann–loschmidt controversy? *Physica A*, 283(1-2):166–170, 2000. ISSN 0378-4371. doi:10.1016/S0378-4371(00)00146-1. URL http://www.sciencedirect.com/science/article/pii/S0378437100001461.

A. Patoz, T. Begušić, and J. Vaníček. On-the-fly ab initio semiclassical evaluation of absorption spectra of polyatomic molecules beyond the condon approximation. *J. Phys. Chem. Lett.*, 9(9): 2367–2372, 2018. doi:10.1021/acs.jpclett.8b00827.

C. Petitjean, D. V. Bevilaqua, E. J. Heller, and P. Jacquod. Displacement echoes: Classical decay and quantum freeze. *Phys. Rev. Lett.*, 98(16):164101, 2007. doi:10.1103/PhysRevLett.98.164101. URL http://link.aps.org/doi/10.1103/PhysRevLett.98.164101.

W. T. Pollard and R. A. Mathies. Analysis of femtosecond dynamic absorption spectra of nonstationary states. *Annu. Rev. Phys. Chem.*, 43(1):497–523, 1992.

W. T. Pollard, H. L. Fragnito, J. Y. Bigot, C. V. Shank, and R. A. Mathies. Quantum-mechanical theory for 6 fs dynamic absorption spectroscopy and its application to nile blue. *Chem. Phys. Lett.*, 168(3-4):239–245, 1990a.

W. T. Pollard, S.-Y. Lee, and R. A. Mathies. Wave packet theory of dynamic absorption spectra in femtosecond pump–probe experiments. *J. Chem. Phys.*, 92(7):4012–4029, 1990b. doi: 10.1063/1.457815. URL http://link.aip.org/link/?JCP/92/4012/1.

M. Quack. Theory of unimolecular reactions induced by monochromatic infrared radiation. *J. Chem. Phys.*, 69:1282–1307, 1978.

M. Quack. Nonlinear intensity dependence of the rate coefficient in unimolecular reactions induced monochromatic by infrared radiation. *Chem. Phys. Lett.*, 65:140–145, 1979.

M. Quack and F. Merkt. *Handbook of High-resolution Spectroscopy*. John Wiley & Sons, 2011.

M. Quack and E. Sutcliffe. On the validity of the quasiresonant approximation for molecular infrared-multiphoton excitation. *J. Chem. Phys.*, 83:3805–3812, 1985.

G. Richings, I. Polyak, K. Spinlove, G. Worth, I. Burghardt, and B. Lasorne. Quantum dynamics simulations using Gaussian wavepackets: the vMCG method. *Int. Rev. Phys. Chem.*, 34(2):269–308, 2015. doi:10.1080/0144235X.2015.1051354.

J. M. Rost. Analytical total photo cross section for atoms. *J. Phys. B*, 28(19):L601, 1995. URL http://stacks.iop.org/0953-4075/28/i=19/a=002.

I. G. Ryabinkin, L. Joubert-Doriol, and A. F. Izmailov. Geometric phase effects in nonadiabatic dynamics near conical intersections. *Acc. Chem. Res.*, 50(7):1785 – 1793, 2017.

K. Saita and D. V. Shalashilin. On-the-fly ab initio molecular dynamics with multiconfigurational ehrenfest method. *J. Chem. Phys.*, 137(22):22A506, 2012. doi:10.1063/1.4734313. URL http://link.aip.org/link/?JCP/137/22A506/1.

G. C. Schatz and M. A. Ratner. *Quantum Mechanics in Chemistry*. Dover Publications, 2002.

L. Seidner, G. Stock, A. L. Sobolewski, and W. Domcke. Ab initio characterization of the S1–S2

conical intersection in pyrazine and calculation of spectra. *J. Chem. Phys.*, 96(7):5298–5309, 1992. ISSN 10897690. doi:10.1063/1.462715.

D. V. Shalashilin and M. S. Child. Real time quantum propagation on a Monte Carlo trajectory guided grids of coupled coherent states: 26D simulation of pyrazine absorption spectrum. *J. Chem. Phys.*, 121(8):3563–3568, 2004. doi:10.1063/1.1776111.

N. E. Shemetulskis and R. F. Loring. Semiclassical theory of the photon echo: Application to polar fluids. *J. Chem. Phys.*, 97(2):1217–1226, 1992. doi:10.1063/1.463248. URL `http://link.aip.org/link/?JCP/97/1217/1`.

Q. Shi and E. Geva. A comparison between different semiclassical approximations for optical response functions in nonpolar liquid solutions. *J. Chem. Phys.*, 122(6):064506, 2005. doi:10.1063/1.1843813. URL `http://link.aip.org/link/?JCP/122/064506/1`.

M. Šulc, H. Hernández, T. J. Martínez, and J. Vaníček. Relation of exact Gaussian basis methods to the dephasing representation: Theory and application to time-resolved electronic spectra. *J. Chem. Phys.*, 139(3):034112, 2013. doi:10.1063/1.4813124.

S. L. Tang, D. G. Imre, and D. Tannor. Ammonia: Dynamical modeling of the absorption spectrum. *J. Chem. Phys.*, 92(10):5919–5934, 1990. doi:10.1063/1.458362.

S. L. Tang, E. H. Abramson, and D. G. Imre. Time-dependent study of the fluorescence spectrum of ammonia. *J. Phys. Chem.*, 95(13):4969–4976, 1991. doi:10.1021/j100166a015. URL `http://pubs.acs.org/doi/abs/10.1021/j100166a015`.

D. J. Tannor. *Introduction to Quantum Mechanics: A Time-Dependent Perspective*. University Science Books, Sausalito, 2007. ISBN 978-1891389238.

J. Tatchen and E. Pollak. Semiclassical on-the-fly computation of the $S_0 \rightarrow S_1$ absorption spectrum of formaldehyde. *J. Chem. Phys.*, 130(4):041103, 2009. doi:10.1063/1.3074100. URL `http://link.aip.org/link/?JCP/130/041103/1`.

M. Thoss, H. Wang, and W. H. Miller. Generalized forward-backward initial value representation for the calculation of correlation functions in complex systems. *J. Chem. Phys.*, 114:9220–9235, 2001.

L. W. Tutt, J. I. Zink, and E. J. Heller. Simplifying the MIME: A formula relating normal mode distortions and frequencies to the MIME frequency. *Inorg. Chem.*, 26(5):2158–2160, 1987. doi:10.1017/CBO9781107415324.004.

R. M. van der Veen, A. Cannizzo, F. van Mourik, A. Vlček, and M. Chergui. Vibrational relaxation and intersystem crossing of binuclear metal complexes in solution. *J. Am. Chem. Soc.*, 133(12):305–315, 2011.

J. Vaníček. Dephasing representation: Employing the shadowing theorem to calculate quantum correlation functions. *Phys. Rev. E*, 70(5):055201, 2004. doi:10.1103/PhysRevE.70.055201. URL `http://link.aps.org/doi/10.1103/PhysRevE.70.055201`.

J. Vaníček. Dephasing representation of quantum fidelity for general pure and mixed states. *Phys.*

Rev. E, 73(4):046204, 2006. doi:10.1103/PhysRevE.73.046204. URL http://link.aps.org/doi/10.1103/PhysRevE.73.046204.

M. Šulc and J. Vaníček. Accelerating the calculation of time-resolved electronic spectra with the cellular dephasing representation. *Mol. Phys.*, 110(9-10):945–955, 2012. doi:10.1080/00268976.2012.668971. URL http://www.tandfonline.com/doi/abs/10.1080/00268976.2012.668971.

A. R. Walton and D. E. Manolopoulos. A new semiclassical initial value method for franck-condon spectra. *Mol. Phys.*, 87(4):961–978, 1996. doi:10.1080/00268979600100651. URL http://www.informaworld.com/10.1080/00268979600100651.

H. Wang and M. Thoss. Multilayer formulation of the multiconfiguration time-dependent hartree theory. *J. Chem. Phys.*, 119(3):1289–1299, 2003. doi:10.1063/1.1580111. URL http://link.aip.org/link/?JCP/119/1289/1.

H. Wang, D. E. Manolopoulos, and W. H. Miller. Generalized filinov transformation of the semiclassical initial value representation. *J. Chem. Phys.*, 115(14):6317–6326, 2001. doi:10.1063/1.1402992. URL http://link.aip.org/link/?JCP/115/6317/1.

M. Wehrle, M. Šulc, and J. Vaníček. Time-resolved electronic spectra with efficient quantum dynamics methods. *Chimia*, 65:334–338, 2011. doi:10.2533/chimia.2011.334. URL http://www.ingentaconnect.com/content/scs/chimia/2011/00000065/00000005/art00012.

M. Wehrle, M. Šulc, and J. Vaníček. On-the-fly ab initio semiclassical dynamics: Identifying degrees of freedom essential for emission spectra of oligothiophenes. *J. Chem. Phys.*, 140(24):244114, 2014.

M. Wehrle, S. Oberli, and J. Vaníček. On-the-fly ab initio semiclassical dynamics of floppy molecules: Absorption and photoelectron spectra of ammonia. *J. Phys. Chem. A*, 119(22):5685, 2015.

S. Y. Y. Wong, D. M. Benoit, M. Lewerenz, A. Brown, and P.-N. Roy. Determination of molecular vibrational state energies using the ab initio semiclassical initial value representation: Application to formaldehyde. *J. Chem. Phys.*, 134(9):094110, 2011. doi:10.1063/1.3553179. URL http://scitation.aip.org/content/aip/journal/jcp/134/9/10.1063/1.3553179.

E. Zambrano, M. Šulc, and J. Vaníček. Improving the accuracy and efficiency of time-resolved electronic spectra calculations: Cellular dephasing representation with a prefactor. *J. Chem. Phys.*, 139(5):054109, 2013. doi:10.1063/1.4817005. URL http://dx.doi.org/10.1063/1.4817005.

S. Zhang and E. Pollak. Monte carlo method for evaluating the quantum real time propagator. *Phys. Rev. Lett.*, 91(19):190201, 2003. doi:10.1103/PhysRevLett.91.190201.

Y. Zhuang, M. R. Siebert, W. L. Hase, K. G. Kay, and M. Ceotto. Evaluating the accuracy of Hessian approximations for direct dynamics simulations. *J. Chem. Theory Comput.*, 9(1):54–64, 2013. doi:10.1021/ct300573h.

T. Zimmermann and J. Vaníček. Communications: Evaluation of the nondiabaticity of quantum molecular dynamics with the dephasing representation of quantum fidelity. *J. Chem. Phys.*, 132

(24):241101, 2010. doi:10.1063/1.3451266. URL http://link.aip.org/link/?JCP/132/241101/1.

T. Zimmermann and J. Vaníček. Measuring nonadiabaticity of molecular quantum dynamics with quantum fidelity and with its efficient semiclassical approximation. *J. Chem. Phys.*, 136(9):094106, 2012a. doi:10.1063/1.3690458. URL http://link.aip.org/link/?JCP/136/094106/1.

T. Zimmermann and J. Vaníček. Evaluation of the importance of spin-orbit couplings in the nonadiabatic quantum dynamics with quantum fidelity and with its efficient "on-the-fly" ab initio semiclassical approximation. *J. Chem. Phys.*, 137(22):22A516, 2012b. doi:10.1063/1.4738878. URL http://link.aip.org/link/?JCP/137/22A516/1.

T. Zimmermann, J. Ruppen, B. Li, and J. Vaníček. Efficient evaluation of the accuracy of molecular quantum dynamics on an approximate analytical or interpolated ab initio potential energy surface. *Int. J. Quant. Chem.*, 110(13):2426–2435, 2010. ISSN 1097-461X. doi:10.1002/qua.22730. URL http://dx.doi.org/10.1002/qua.22730.